Article:
West, R and Mobilia, M (2020) Fixation properties of rock-paper-scissors games in fluctuating populations. Journal of Theoretical Biology, 491. 110135. ISSN: 0022-5193

https://doi.org/10.1016/j.jtbi.2019.110135

Fixation properties of rock-paper-scissors games in fluctuating populations

Robert West and Mauro Mobilia

Department of Applied Mathematics, School of Mathematics, University of Leeds, Leeds LS2 9JT, United Kingdom

Abstract

Rock-paper-scissors games metaphorically model cyclic dominance in ecology and microbiology. In a static environment, these models are characterized by fixation probabilities obeying two different "laws" in large and small well-mixed populations. Here, we investigate the evolution of these three-species models subject to a randomly switching carrying capacity modeling the endless change between states of resources scarcity and abundance. Focusing mainly on the zero-sum rock-paper-scissors game, equivalent to the cyclic Lotka-Volterra model, we study how the *coupling* of demographic and environmental noise influences the fixation properties. More specifically, we investigate which species is the most likely to prevail in a population of fluctuating size and how the outcome depends on the environmental variability. We show that demographic noise coupled with environmental randomness "levels the field" of cyclic competition by balancing the effect of selection. In particular, we show that fast switching effectively reduces the selection intensity proportionally to the variance of the carrying capacity. We determine the conditions under which new fixation scenarios arise, where the most likely species to prevail changes with the rate of switching and the variance of the carrying capacity. Random switching has a limited effect on the mean fixation time that scales linearly with the average population size. Hence, environmental randomness makes the cyclic competition more egalitarian, but does not prolong the species coexistence. We also show how the fixation probabilities of close-to-zero-sum rock-paper-scissors games can be obtained from those of the zero-sum model by rescaling the selection intensity.

Keywords: Population Dynamics, Ecology and Evolution, Fluctuations, Stochastic Processes, Rock-Paper-Scissors
PACS: 05.40.-a, 87.23.Kg, 02.50.Ey, 87.23.-n

1. Introduction

Studying what affects the extinction and survival of species in ecosystems is of paramount importance [1]. It is well known that birth and death events cause demographic fluctuations (internal noise, IN) that can ultimately lead to species extinction and fixation – when one species takes over the entire population [2, 3]. IN being stronger in small communities than in large populations, various survival and fixation scenarios arise in populations of different size and structure [4, 5, 6, 7, 8, 9]. For instance, experiments on a colicinogenic microbial communities have demonstrated that cyclic rock-paper-scissors-like competition between three strains leads to intriguing behavior [10]: the colicin-resistant strain is the only one to survive in a large well-mixed population, whereas all species coexist for a long time on a plate. These observations, and the rock-paper-scissors being the paradigmatic model of cyclic dominance in ecology and microbiology, see, *e.g*, Refs. [11, 12, 14, 16, 15, 17, 9, 18], have motivated the study of the survival/fixation properties of the cyclic Lotka-Volterra model (CLV). This is characterized by a zero-sum rock-paper-scissors competition between three species [14, 15, 17, 5, 4, 19, 21, 6, 22, 23, 24, 25, 26, 27, 28, 30, 31, 32, 33]. Remarkably, it has been shown that, when the population size is *constant*, the fixation probabilities in the CLV obey two simple laws [6, 4, 23]: In a large well-mixed population, the species receiving the lowest payoff is the most likely to survive and fixate, a result referred to as the "law of the weakest", whereas a different law, called the "law of stay out", arises in smaller populations.

In fact, the fate of a population is influenced by numerous endlessly changing environmental conditions (e.g. light, pH, temperature, nutrient abundance) [34]. Detailed knowledge about exogenous factors being generally unknown, these are often modeled as environmental (external) noise (EN) [35, 36, 37, 25, 38, 39, 40, 41, 42, 43, 44, 45, 33, 46, 47]. In many biological applications the population size varies in time due

to changing external factors [48, 49]. The EN-caused fluctuations in the population size in turn affect the demographic fluctuations which results in a coupling of IN and EN leading to feedback loops that shape the population's long-term evolution [50, 51, 52, 53, 54, 55, 56, 57, 58]. This is particularly relevant in microbial communities that are subject to sudden and extreme environmental changes leading, *e.g.*, to population bottelnecks or to the collapse of biofilms [59, 60, 61, 62]. While EN and IN are naturally interdependent in many biological applications, the theoretical understanding of their coupling is still limited. Recently, progress has been made in simple two-species models [56, 57], but the analysis of EN and IN coupling in populations consisting of many interacting species is a formidable task.

Here, we study the *coupled effect* of environmental and internal noise on the fixation properties of three-species rock-paper-scissors games in a population of *fluctuating size*, when the resources continuously vary between states of scarcity and abundance. Environmental randomness is modelled by assuming that the population is subject to a carrying capacity, driven by a dichotomous Markov noise [63, 64, 65, 66], randomly switching between two values. A distinctive feature of this model is the coupling of demographic noise with environmental variability: Along with the carrying capacity, the population size can fluctuate and switch between values dominated by either the law of the weakest or stay out. It is therefore a priori not clear which species will be the most likely to prevail and how the outcome depends on the environmental variability. Here, we show that environmental variability generally balances the effect of selection and can yield novel fixation scenarios.

The models considered in this work are introduced in Sec. 2. Section 3 is dedicated to the analysis of the long-time dynamics of the cyclic Lotka-Volterra model (CLV) with a constant carrying capacity. This paves the way to the detailed study of the survival and fixation properties in the CLV subject to a randomly switching carrying capacity presented in Sec. 4. In Section 5, our results are extended to close-to-zero-sum rock-paper-scissors games. Our conclusions are presented in Sec. 6. Technical details and supporting information are provided in an accompanying supplementary material (SM) [85]. Thereafter, S*a.b* and S*c* refer to the section *a.b* and equation or figure S*c* in the SM [85].

2. Rock-paper-scissors games with a carrying capacity

We consider a well-mixed population (no spatial structure) of fluctuating size $N(t)$ containing three species, denoted by 1, 2, and 3. At time t, the population consists of $N_i(t)$ individuals of species $i \in \{1, 2, 3\}$, such that $N(t) = N_1(t) + N_2(t) + N_3(t)$. As in all rock-paper-scissors (RPS) games [14, 15, 16, 17], species are engaged in a cyclic competition: Species 1 dominates over type 2, which outcompetes species 3, which in turn wins against species 1 closing the cycle. In a game-theoretic formulation, the underpinning cyclic competition can be generically described in terms of the payoff matrix [13, 14, 15, 16, 17, 18, 67, 68, 69]:

$\mathcal{P} =$

Species	1	2	3
1	0	r_1	$-r_3(1+\epsilon)$
2	$-r_1(1+\epsilon)$	0	r_2
3	r_3	$-r_2(1+\epsilon)$	0

Here, $0 < r_i = O(1)$, with $\sum_i^3 r_i = 1$, and $\epsilon > -1$. According to $\mathcal{P}$, an i-individual gains a payoff r_i against an $(i+1)$-individual and gets a negative payoff $-r_{i-1}(1+\epsilon)$ against an $(i-1)$-player (with cyclic ordering, i.e. $1-1 \equiv 3$ and $3+1 \equiv 1$, see below). Hereafter, species $i-1$ is therefore referred to as the "strong opponent" of type i, whereas species $i+1$ is its "weak opponent". Interactions between individuals of same species do not provide any payoff. When $\epsilon = 0$, $\mathcal{P}$ underlies a zero-sum RPS game, also referred to as "cyclic Lotka-Volterra model" (CLV) [22, 24, 23, 4, 5, 13, 14, 15, 19, 21, 6, 25, 26, 27, 29, 30, 31, 32, 28, 33, 18]: what i gains is exactly what $i+1$ loses. When $\epsilon \neq 0$, $\mathcal{P}$ describes the general, non-zero-sum, RPS cyclic competition: What an i loses against $i-1$, $r_{i-1}(1+\epsilon)$, differs from the payoff r_{i-1} received by $i-1$ against i, see, *e.g.*, [20, 67, 68, 69, 18, 9, 8, 70, 71, 72, 73, 74, 75, 76, 77]. In Secs. 3 and 4, we focus on the CLV, and then discuss close-to-zero-sum RPS games ($|\epsilon| \ll 1$) in Sec. 5.

In terms of the densities $x_i \equiv N_i/N$ of each species in the population, that span the phase space simplex S_3 [6, 33], species i's expected payoff is

$$\begin{aligned} \Pi_i &= (\mathcal{P}\vec{x})_i = r_i x_{i+1} - r_{i-1}(1+\epsilon)x_{i-1}, \qquad (1) \\ \bar{\Pi} &= \vec{x}\cdot\mathcal{P}\vec{x} = -\epsilon\sum_{i=1}^{3} r_i x_i x_{i+1}, \end{aligned}$$

where $\vec{x} = (x_1, x_2, x_3)$ and $\bar{\Pi}$ is the population's average payoff which vanishes when $\epsilon = 0$ (zero-sum game). Here and in the following, the indices are ordered cyclically: In Eq. (1), $x_{1-1} \equiv x_3, r_{1-1} \equiv r_3$ and $x_{3+1} \equiv x_1, r_{3+1} \equiv r_1$. In evolutionary game theory, it is common to define the fitness f_i of species i as a linear function of the expected payoff Π_i [14, 15, 16, 17]:

$$f_i = 1 + s\Pi_i \quad \text{and} \quad \bar{f} = 1 + s\bar{\Pi} \quad \text{(average fitness)}, \quad (2)$$

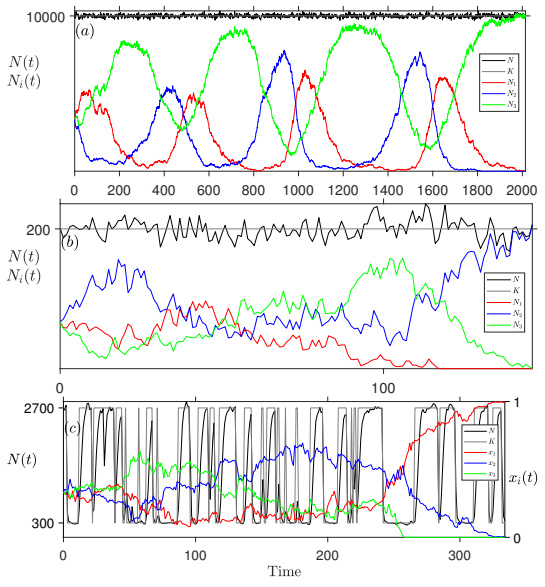

Figure 1: (a,b) Sample paths of $N(t)$ (black), and $N_i(t)$ (colored) with constant carrying capacity $K = 10^4$ in (a) and $K = 200$ in (b); solid gray lines show $N(t) = K$. Parameters are $(s, r_1, r_2, r_3) = (1/10, 3/5, 1/5, 1/5)$. $N(t)$ quickly fluctuates about K, while N_i evolve on a much slower timescale, see text. Fluctuations and extinction properties vary with sK, see Sec. 3. (c) Sample paths of $N(t)$ (black), densities $x_i(t) = N_i(t)/N(t)$ (colored), and typical evolution of the randomly switching $K(t)$ (gray). Parameters are: $(s, r_1, r_2, r_3, \nu, K_+, K_-) = (1/20, 1/3, 1/3, 1/3, 1/4, 2700, 300)$. $N(t)$ quickly settles into its (quasi) stationary state while x_i vary much more slowly until fixation occurs in a time $\sim \langle K \rangle$, see Sec. 4.2. In all panels: $N_1(t), x_1(t)$ in red, $N_2(t), x_2(t)$ in blue, and $N_3(t), x_3(t)$ in green, $\epsilon = 0$. Initially, all species have the same density $1/3$.

where $s > 0$ is a parameter measuring the contribution to the fitness arising from $\mathcal{P}$, i.e. the "selection intensity": species have close fitness in the biologically relevant case $s \ll 1$ (weak selection), whereas the fitness fully features the cyclic dominance when $s = O(1)$ (strong selection). The average fitness $\bar{f} = \sum_{i=1}^{3} x_i f_i = 1$ in the CLV ($\epsilon = 0$).

Population dynamics is often modeled by assuming a finite population of *constant size* evolving according to a Moran process [78, 3, 79, 80, 15], see Sec. S1. Here, the population size is *not constant but fluctuates in time* due to environmental variability modeled by introducing a carrying capacity K, see Fig. 1. Below, we first consider a constant carrying capacity, and then focus on the case where K fluctuates in time. For the fluctuating carrying capacity, we assume that $K(t)$ continuously switches between two values, K_+ and K_-. This simply models that available resources continuously and randomly change from being scarce ($K = K_-$) to being abundant ($K = K_+ > K_-$). The population size thus varies with K and so do the demographic fluctuations, resulting in of IN being *coupled* to EN. For simplicity, we model the switches of $K(t)$ with a *colored dichotomous Markov noise* [64, 63], or "random telegraph noise", $\xi(t) \in \{-1, +1\}$ with symmetric switching rate ν:

$$\xi \xrightarrow{\nu} -\xi. \tag{3}$$

Here, the dichotomous noise is always at stationarity [1]: Its average vanishes, $\langle \xi(t) \rangle = 0$, and its autocorrelation is $\langle \xi(t)\xi(t') \rangle = \exp(-2\nu|t - t'|)$ [64, 63] (here, $\langle \cdot \rangle$ denotes the ensemble average over the environmental noise). The randomly switching carrying capacity therefore reads [56, 57]

$$K(t) = \frac{1}{2}\left[(K_+ + K_-) + \xi(t)(K_+ - K_-)\right], \tag{4}$$

where $\langle K \rangle = (K_+ + K_-)/2$ is its constant average. The constant-K case is recovered by setting $K_+ = K_-$ in (4).

In what is arguably its simplest formulation, see Sec. S1, the RPS dynamics subject to $K(t)$ is here defined in terms of the birth-death process [51, 56]

$$N_i \xrightarrow{T_i^+} N_i + 1 \quad \text{and} \quad N_i \xrightarrow{T_i^-} N_i - 1, \tag{5}$$

for the birth ($N_i \to N_i + 1$) and death ($N_i \to N_i - 1$) of an i-individual, respectively, with the transition rates

$$T_i^+ = f_i N_i \quad \text{and} \quad T_i^- = \frac{N}{K(t)} N_i, \tag{6}$$

where the randomly switching carrying capacity is given by (4), while $K(t) = K$ when the carrying capacity is constant. It is worth noting that we consider $0 \le s \le 1/(1 + \epsilon)$, which suffices to ensure $T_i^{\pm} \ge 0$. The master equation associated with the continuous-time birth-death process (5),(6) gives the probability $P(\vec{N}, \xi, t)$ to find the population in state $(\vec{N}, \xi) = (N_1, N_2, N_3, \xi)$ at time t [82, 83], and reads:

$$\begin{aligned} \frac{dP(\vec{N},\xi,t)}{dt} &= \sum_{i=1}^{3} (\mathbb{E}_i^- - 1)\left[T_i^+ P(\vec{N},\xi,t)\right] \\ &+ \sum_{i=1}^{3} (\mathbb{E}_i^+ - 1)\left[T_i^- P(\vec{N},\xi,t)\right] \\ &+ \nu\left[P(\vec{N},-\xi,t) - P(\vec{N},\xi,t)\right], \end{aligned} \tag{7}$$

where $\mathbb{E}_i^{\pm}$ are shift operators, associated with (5), such that $\mathbb{E}_1^{\pm} h(N_1, N_2, N_3, t) = h(N_1 \pm 1, N_2, N_3, t)$ etc, for any $h(\vec{N}, \xi, t)$, and the last line accounts for the random switching of K. In Eq (7), $P(\vec{N}, \xi, t) = 0$ whenever any

[1] In all our simulations, without loss of generality, $N(0) = 2K_+K_-/(K_+ + K_-)$.

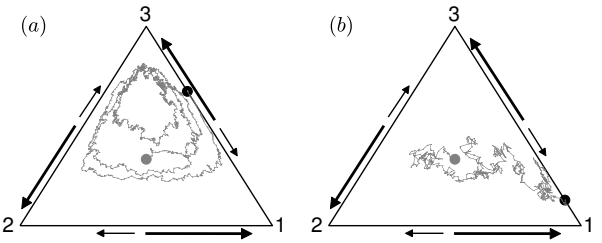

Figure 2: Stochastic orbits in S_3 of the constant-K BDCLV ($\epsilon = 0$) of Fig. 1 (a,b), with $(s, r_1, r_2, r_3) = (1/10, 3/5, 1/5, 1/5)$ and illustration of Stages 1 and 2 of dynamics, see text. Initially all species have the same density 1/3 (gray dot), and (a) $K = 10^4$, (b) $K = 200$. (a) In Stage 1, when $sK \gg 1$, erratic trajectories approach ∂S_3 from the outermost orbit (deterministic orbit at a distance $1/K$ from ∂S_3, see text). (b) When $sK = O(10)$, in Stage 1, stochastic trajectories reach ∂S_3 without settling onto the outermost orbit. Stage 2: Once on an edge of ∂S_3 (black dot), a competition (shown as arrows) takes place between species i and its weak opponent $i + 1$, with the former (long arrows) more likely to win than the latter (short arrows), see text.

$N_i < 0$. This multidimensional master equation can be simulated exactly to fully capture the stochastic RPS dynamics [84]. This is characterized by a first stage in which all species coexist, then two species compete in a second stage, and, after a time that diverges with the system size, the population finally collapses [2]. Here, we focus on the first two stages of the dynamics in which $N(t)$ is characterized by its quasi-stationary distribution (N-QSD). In the constant-K case, one drops the last line and sets $K_+ = K_- = K$ in Eq. (7), yielding the underpinning master equation for $P(\vec{N}, t)$.

3. The birth-and-death cyclic Lotka-Volterra model ($\epsilon = 0$) with constant carrying capacity

In order to understand how environmental variability affects the RPS dynamics, it is useful to study first the dynamics of the model defined by (1)-(6) with $\epsilon = 0$ when the carrying capacity K is constant. This zero-sum model ($\bar{\Pi} = 0, \bar{f} = 1$), is referred to as the constant-K birth-and-death cyclic Lotka-Volterra model (BDCLV) and its dynamics is fully described by the underpinning ME. Proceeding as in Sec. S1, the mean-field description of the constant-K BDCLV is obtained by neglecting all fluctuations, yielding

$$\dot{N} = \sum_{i=1}^{3}(T_i^+ - T_i^-) = N\left(1 - \frac{N}{K}\right), \quad (8)$$

$$\dot{x}_i = \frac{T_i^+ - T_i^-}{N} - x_i\frac{\dot{N}}{N} = x_i[\alpha_i x_{i+1} - \alpha_{i-1}x_{i-1}], \quad (9)$$

where $\alpha_i \equiv sr_i$, and the dot stands for the time derivative. Clearly, the population size obeys the logistic equation (8), and thus $N(t) \to K$ after a time $t = O(1)$. The rate equations for $x_i = N_i/N$ describe how the population composition changes due to cyclic dominance on a timescale $1/s$. Eqs. (8) and (9) are decoupled and, when $s \ll 1$, there is a timescale separation: N rapidly approaches K while the x_i's evolve much slower. When time is rescaled ($t \to st$), the rate equations (9) coincide with the celebrated replicator equations of the zero-sum RPS game [13, 14, 15, 16, 17]. These are characterized by a neutrally stable fixed point $\vec{x}^* = (r_2, r_3, r_1)$ associated with the coexistence of a fraction r_{i+1} of each species i, and three saddle (unstable) fixed points $\{\vec{e}_1 = (1, 0, 0), \vec{e}_2 = (0, 1, 0), \vec{e}_3 = (0, 0, 1)\}$, $\vec{e}_i$ corresponding to a state in which only individuals of species i are present. In addition to conserving $x_1 + x_2 + x_3 = 1$, Eqs. (9) also conserve the quantity $\mathcal{R} = \prod_{i=1}^{3} x_i^{r_{i+1}}$. The deterministic trajectories in the phase space S_3 are therefore neutrally stable orbits surrounding $\vec{x}^*$ [14]. The dynamics in a finite population is characterized by noisy oscillations about $\vec{x}^*$, see Fig. 1 (a,b), with erratic trajectories performing a random walk between the deterministic orbits until ∂S_3 is hit and one species goes extinct. This first stage of the dynamics (Stage 1) where the three species coexist is followed by Stage 2 where the two surviving species, say i and $i + 1$, compete along the edge $(i, i + 1)$ of S_3 until one them prevails and fixates, see Fig. 2. The population size $N(t)$ is not constant but, after $t = O(1)$, fluctuates about K, with fluctuation intensity that decreases with K, see Fig. 1 (a,b). It is worth noting that the population size keeps fluctuating, $N(t) \approx K$, even after Stage 2 when it consists of only the species having fixated in Stage 2, see Footnote 2.

The fact that, after a short transient, $N(t) \approx K$ suggests a relation between the constant-K BDCLV and the cyclic Lotka-Volterra model evolving according to a Moran process in a population of constant size $N = K$ [67, 16, 68, 69], see Sec. S1.2. In the Moran cyclic Lotka-Volterra model (MCLV), the birth of an i-individual and the death of an individual of type $j \neq i$ occurs simultaneously: In the MCLV, an i replaces a j with rate $T_{j\to i}$ and the population size remains constant, see, *e.g.*, [67, 68, 69]. In Sec. S1.2, the constant-K BD-

[2] The population eventually collapses into the unique absorbing state of the birth-death process (5)-(7) which is $N = N_i = 0$. However, this phenomenon is practically unobservable in a population with a large carrying capacity: it occurs after lingering in the N-QSD for a time that diverges with the system size [81], and is here ignored.

CLV is shown to have the same fixation properties as the MCLV with transition rates $T_{j\to i} = T_i^+ T_j^-/K$ and $N = K$, see Fig. S1.

It is also useful to compare the constant-K BDCLV with the so-called chemical cyclic Lotka-Volterra model (cCLV), see Sec. S1.3. In the cCLV, the cyclic competition between the three species is of predator-prey type: An i-individual (predator) kills an $(i+1)$-individual (its prey) and immediately replace it, leaving the population size constant. In Sec. S1.3, we show that the cCLV admits the same mean-field dynamics as the constant-K BDCLV, see Eq. (S15). However, once a species has gone extinct in the cCLV, there is a predator-prey competition in Stage 2 won by the predator with a probability 1. Hence, Stage 1 survival and fixation probabilities coincide in the cCLV. Remarkably, it was found that these quantities obey two simple laws, the so-called "law of the weakest" (LOW) when N is large and the "law of stay out" (LOSO) in smaller populations [6, 4, 33], see Sec. S1.3.1 and Fig. S2.

As detailed in Sec. S2, the stage 1 dynamics of the constant-K BDCLV is similar to the stage 1 cCLV dynamics in a population of size $O(sK)$. The stage 2 dynamics in the constant-K BDCLV and MCLV with $N = K$ are similar, with both surviving species having a non-zero probability to fixate, see Sec. S2.

In what follows, we exploit the relationships between the BDCLV and the MCLV and cCLV to shed light on its fixation properties when K is constant and randomly switching. In particular, we study the novel survival scenarios that can arise when $N(t)$ fluctuates.

3.1. Survival, absorption and fixation probabilities in the constant-K BDCLV

All three species coexist during Stage 1: In the constant-K BDCLV their fractions erratically oscillate about $\vec{x}^*$ until ∂S_3 is hit, see Figs. 1 (a,b) and 2. Stage 1 ends at this point and is characterized by the probability $\phi_{i,i+1}$ to have reached the edge $(i, i+1)$ (survival of species i and $i+1$) or, equivalently, that species $i-1$ is the first to die out. Once on ∂S_3, Stage 2 starts and two species, say i and $i+1$, compete along their edge until either i, with probability ϕ_i, or $i+1$, with probability $1-\phi_i$, get absorbed. Clearly, the stage 2 dynamics is conditioned by the outcome of Stage 1 and the overall fixation probability $\widetilde{\phi_i}$ depends on $\phi_{i,j}$ and ϕ_i, see Eq. (16).

Below, we show that $\phi_{i,i+1}, \phi_i$ and $\widetilde{\phi_i}$ are functions of sK, see Figs. 3 and 4, and can respectively be inferred from the well-known properties of the cCLV and MCLV, see Sec. S1. In our discussion, we distinguish three regimes: (i) *quasi-neutrality*, when $sK \ll 1$ and $K \gg 1$; (ii) *weak selection*, when $sK = O(10)$, with $s \ll 1$ and $K \gg 1$; and (iii) *strong selection*, when $sK \gg 1$, with $s = O(1)$ and $K \gg 1$. In the examples below, these three regimes are identified as follows: $s \lesssim 1/K$ in regime (i), $1/K \lesssim s \lesssim 100/K$ in regime (ii), and $s \gtrsim 100/K$ in regime (iii), with $K \gg 1$. Furthermore, since the overall fixation probability of each species $\widetilde{\phi_i}$ is trivially $1/3$ when $r_1 = r_2 = r_3 = 1/3$ [19, 6, 33], we focus on the general case where the r_i's are unequal. All figures have been obtained with the initial fraction $1/3$ of each species, i.e. $\vec{x}_0 \equiv (x_1(0), x_2(0), x_3(0)) = \vec{x}_c \equiv (1,1,1)/3$, and we consider the following set of parameters: $\vec{r} \equiv (r_1, r_2, r_3) = \vec{r}^{(1)} \equiv (1,5,5)/11$ and $\vec{r} = \vec{r}^{(2)} \equiv (3,1,1)/5$. These choices suffice to reveal most of the generic properties of the system. When we study how $\phi_{i,i+1}, \phi_i$ and $\widetilde{\phi_i}$ depend on sK, in Figs. 3 and 4 we consider $K \in \varkappa \equiv \{1000, 450, 250, 90, 50\}$ and $s = 1$ for $K = 1000$, $s \in \{10^{-k/4}, k = 0\dots3\}$ for $K = 450$, $s \in \{10^{-(2+k)/4}, k = 0\dots9\}$ for $K = 250$, $s \in \{10^{-k/4}, k = 0\dots8\}$ for $K = 90$, and $s \in \{10^{-(9+k)/4}, k = 0\dots3\}$ for $K = 50$. In all figures (except Figs. 1 and 2), simulation results have been sampled over $10^4 - 10^5$ realizations.

3.1.1. Stage 1: Survival probabilities in the constant-K BDCLV

The stage 1 dynamics of the constant-K BDCLV and cCLV with $N = O(sK)$ are similar, see Sec. S2. The constant-K BDCLV survival probabilities $\phi_{i,j}$ are therefore similar to the survival/fixation probabilities in the cCLV. These obey the LOW when N is large and the LOSO in smaller populations [6, 4, 33], see Sec. S1.3.1. The LOW and LOSO are here used to determine $\phi_{i,j}$ in regimes (ii) and (iii).

- Regime (i): When $sK \ll 1$, with $K \gg 1$, the system is at quasi-neutrality. The dynamics is driven by demographic fluctuations and all species have the same survival probability $\phi_{i,i+1} \approx 1/3$, see (i) in Fig. 3 (a,b).

- Regime (ii): When $sK = O(10)$ and $K \gg 1$, the intensity of selection strength is weak ($s \ll 1$) and comparable to that of demographic fluctuations. From the relation with the cCLV, we infer that $\phi_{i,i+1}$ is given by the fixation probability $\phi_i^{\mathrm{cCLV}}|_{sK}$ of species i in the cCLV in a population of size of order sK, i.e. $\phi_{i,i+1} \approx \phi_i^{\mathrm{cCLV}}|_{sK}$. In regime (ii), $\phi_i^{\mathrm{cCLV}}|_{sK}$ obeys the LOSO, see Sec. S1.3.1, and from Eq. (S.20) we obtain:

$$\begin{aligned} &\phi_{i-1,i} > \phi_{i,i+1}, \phi_{i+1,i-1} \quad \text{if} \quad r_i > r_{i\pm1} \\ &\phi_{i,i+1} \approx \phi_{i+1,i-1} > \phi_{i-1,i} \quad \text{if} \quad r_{i+1} = r_{i-1} > r_i. \end{aligned} \tag{10}$$

Accordingly, when $r_i > r_{i\pm1}$ species $i-1$ and i are the most likely to survive Stage 1 under weak selection, as confirmed by Fig. 3 (b). When $r_{i+1} = r_{i-1} > r_i$ and

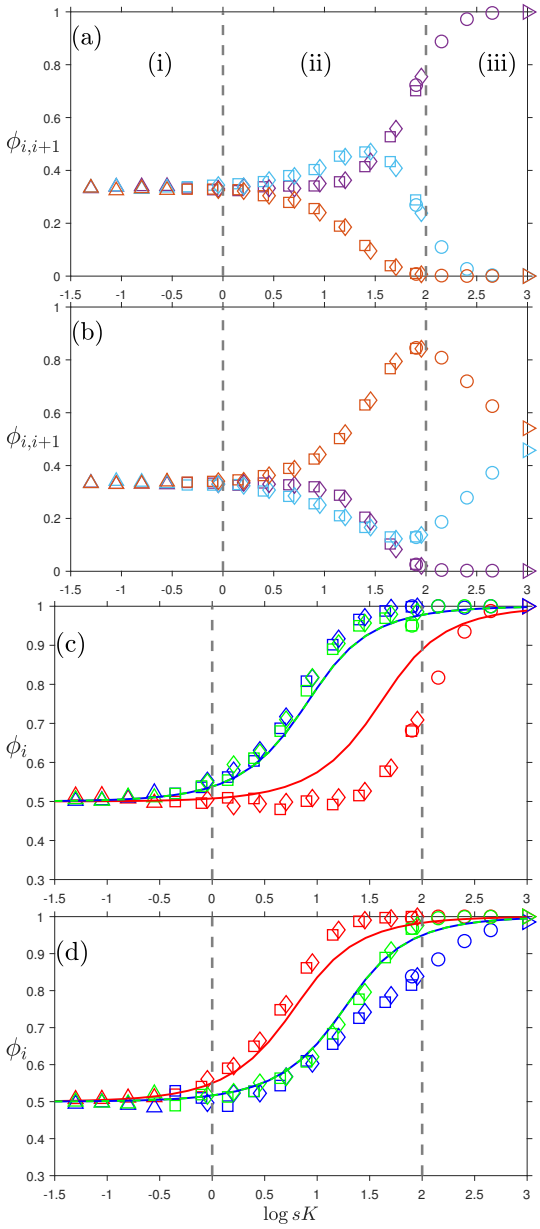

Figure 3: (a,b) Constant-K BDCLV survival probabilities simulation results ($\Diamond$): $\phi_{1,2}$ (purple), $\phi_{2,3}$ (light blue) and $\phi_{3,1}$ (orange) vs. sK for values of $s \in (10^{-3}, 1)$ and $K \in \varkappa$ in regimes (i)-(iii) separated by dashed lines, see text. Non-monotonicity arises across regimes (ii) and (iii) and can be explained in terms of the LOSO (regime (ii)) and LOW (regime (iii)), see text. (a) $\vec{r} = \vec{r}^{(1)}$; species 1 and 3 are the most likely to die out in regime (ii) and (iii), respectively. (b) $\vec{r} = \vec{r}^{(2)}$; species 2 and 1 are the most likely to die out in regime (ii) and (iii), respectively. (c,d) Constant-K BDCLV absorption probabilities ϕ_i vs. sK: ϕ_1 (red), ϕ_2 (blue) and ϕ_3 (green) vs. sK for $K = (1000, 450, 250, 50, 20)$, with (c) $\vec{r} = \vec{r}^{(1)}$ and (d) $\vec{r} = \vec{r}^{(2)}$. The solid line is given by (15) and coincide for species 2 and 3. In all panels $K = 1000$ ($\triangleright$), 450 ($\circ$), 250, ($\diamond$), 90 ($\square$), 50 ($\triangle$), $\epsilon = 0$, $\vec{x}_0 = \vec{x}_c$.

$sK = O(10)$, the edges $(i, i+1)$ and $(i+1, i-1)$ are the most likely to be hit, while species $i-1$ is most likely to die out first, see Fig. 3 (a). While the $\phi_{i,j}$'s obey the LOSO, we notice that $\phi_{i,j} \approx 1/3$ when $s \ll 1$.

- Regime (iii): When $sK \gg 1$, with $s = O(1)$ and $K \gg 1$, the stage 1 dynamics is governed by cyclic dominance. An edge of S_3 is hit from the system's outermost orbit as in the cCLV, see Sec. S2 and Fig. 2 (a). From the relation between the constant-K BDCLV and the cCLV, we have $\phi_{i,i+1} \approx \phi_i^{\text{cCLV}}|_{sK}$ which obeys the LOW in regime (iii), and therefore from Eq. (S18) we have:

$$\begin{aligned} &\phi_{i,i+1} > \phi_{i+1,i-1}, \phi_{i-1,i} \text{ if } \quad r_i < r_{i\pm1}, \\ &\phi_{i,i+1} \approx \phi_{i+1,i-1} > \phi_{i-1,i} \text{ if } \quad r_i = r_{i+1} < r_{i-1}. \end{aligned} \tag{11}$$

When $sK \gtrsim 10^3$, the LOW becomes asymptotically a zero-one law: $\phi_{i,i+1} \to 1, \phi_{i-1,i} \to 0$ and $\phi_{i+1,i-1} \to 0$ if $r_i < r_{i\pm1}$, and $\phi_{i,i+1} = \phi_{i+1,i-1} \to 1/2, \phi_{i-1,i+1} \to 0$ if $r_i = r_{i+1} < r_{i-1}$, see Eq. (S.19). Accordingly, when $sK \gg 1$ and $r_i < r_{i\pm1}$ species i and $i+1$ are most likely to survive and species $i-1$ the most likely to die out in Stage 1, in agreement with Fig. 3 (a).

The relations (10) and (11) explain that $\phi_{i,i+1}$ is a function of sK that can exhibit a non-monotonic behavior. For instance, for $\vec{r} = \vec{r}^{(1)}$ as in Fig. 3 (a), the relations (10) yield $\phi_{1,2} \approx \phi_{2,3} > \phi_{3,1}$ when $sK = O(10)$, and (11) predict $\phi_{1,2} > \phi_{2,3}, \phi_{3,1}$ when $sK \gg 1$, while $\phi_{1,2} \approx \phi_{2,3} \approx \phi_{3,1} \approx 1/3$ when $sK \ll 1$. From these results, it is clear that $\phi_{2,3}$ increases across the regimes (i)-(ii), and then decreases with sK across the regimes (ii)-(iii), whereas $\phi_{1,2}$ and $\phi_{3,1}$ respectively increases and decreases with sK across all regimes.

3.1.2. *Stage 2: Absorption probabilities in the constant-K BDCLV*

At start of Stage 2, species i competes against $i+1$ (weak opponent), along the edge $(i, i+1)$ where their fitnesses are $f_i = 1 + \alpha_i(1 - x_i)$ and $f_{i+1} = 1 - \alpha_i x_i$, see (2). Stage 2 ends with the absorption of either i or $i+1$, respectively with probability ϕ_i and $1 - \phi_i$.

- At quasi neutrality, species i's selective advantage is negligible since $f_i - f_{i+1} = \alpha_i \ll 1$. In regime (i), species i and $i+1$ have therefore almost the same absorption probability $\phi_i \approx 1/2$.

- Under strong selection, species i has an important selective advantage over species $i+1$: $f_i - f_{i+1} = O(1)$. In regime (iii), species i is almost certain to be absorbed as in Stage 2 of the cCLV dynamics, and therefore $\phi_i \approx 1$ as predicted by the LOW, see Secs. S1.3 and S2.

- Under weak selection, in regime (ii), ϕ_i is nontrivial and can be obtained from the fixation probability $\phi_i|_K$ of species i in the MCLV with $N = K$, see Appendices Secs. S1.2 and S3. When the stage 2 dynamics starts with a fraction $\hat{x}_i$ of individuals of species i, $\phi_i|_K$ under weak selection is obtained from the backward Fokker-Planck generator

$$\mathcal{G}_{(i,i+1)}|_K = \frac{x_i(1-x_i)}{K}\left[K\alpha_i \frac{d}{dx_i} + \frac{d^2}{dx_i^2}\right], \tag{12}$$

by solving $\mathcal{G}_{(i,i+1)}|_K(\hat{x}_i)\phi_i|_K(\hat{x}_i) = 0$ with $\phi_i|_K(1) = 1 - \phi_i|_K(0) = 1$, see Eq. (S24), yielding

$$\phi_i \simeq \phi_i(\hat{x}_i)|_K = \frac{1 - e^{-\alpha_i K \hat{x}_i}}{1 - e^{-\alpha_i K}}. \tag{13}$$

A difficulty arises from $\hat{x}_i$ being a random variable depending on the outcome of Stage 1: $\hat{x}_i$ is distributed according to the probability density $P_{(i,i+1)}(\hat{x}_i)$. The absorption probability is thus obtained by averaging (13) over $P_{(i,i+1)}$:

$$\phi_i \simeq \phi_i|_K = \int_0^1 P_{(i,i+1)}(\hat{x}_i)\, \phi_i(\hat{x}_i)|_K \, d\hat{x}_i. \tag{14}$$

In practice, $P_{(i,i+1)}(\hat{x}_i)$ is obtained from stochastic simulations, see Sec. S4. Analytical progress can be made by noticing that in regime (ii) where $s \ll 1$ and $sK \lesssim 10$, each pair $i, i+1$ has approximately the same survival probability at the end of Stage 1 ($\phi_{i,i+1} \approx 1/3$, see Fig. 3 (a,b)), and the initial distribution along $(i, i+1)$ can be assumed to be uniform, i.e. $P_{i,i+1}(\hat{x}_i) \approx 1$, see Fig. S3. Substituting in Eq. (14), we obtain the approximation ($s \ll 1, sK \lesssim 10$):

$$\phi_i \simeq \phi_i|_K \approx \frac{e^{-\alpha_i K} + \alpha_i K - 1}{\alpha_i K(1 - e^{-\alpha_i K})}, \tag{15}$$

which is an S-shaped function of $\alpha_i K$ that correctly predicts the behaviors $\phi_i \to 1/2$ when $\alpha_i K \ll 1$ (regime (i)) and $\phi_i \to 1$ when $\alpha_i K \gg 1$ (regime (iii)), see Fig. 3 (c,d). Comparison with simulation results of Fig. 3 (c,d) confirm that ϕ_i is sigmoid function of sK and Eq. (15) provides a good approximation of ϕ_i when the assumption $P_{(i,i+1)} \approx 1$ holds, see Fig. S3.

3.1.3. *Total fixation probabilities in the constant-K BD-CLV*

Species i's total fixation probability $\widetilde{\phi}_i$ consists of two contributions: $\phi_{i,i+1}\phi_i$ and $\phi_{i-1,i}(1 - \phi_{i-1})$. The first one counts the probability for i to fixate after hitting the edge $(i, i+1)$, with a probability $\phi_{i,i+1}$, and prevailing against $i+1$ (weak opponent) with a probability ϕ_i. We also

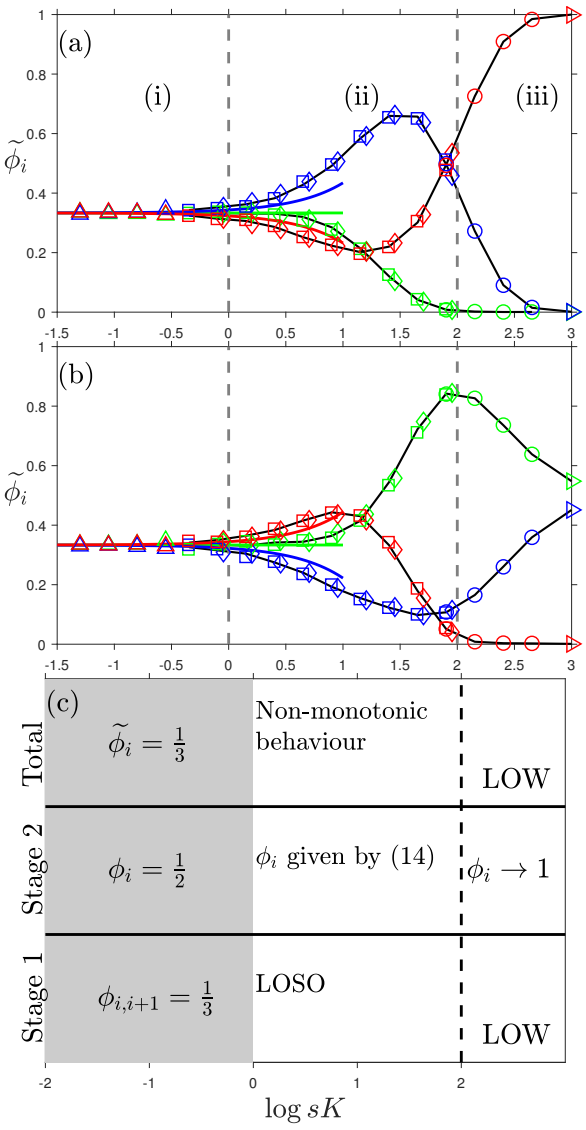

Figure 4: (a,b) Total fixation probabilities $\widetilde{\phi}_1$ (red), $\widetilde{\phi}_2$ (blue), $\widetilde{\phi}_3$ (green) vs. sK for values of $s \in (10^{-3}, 1)$ and $K \in \varkappa$ with symbols as in Fig. 3, see text. Regimes (i)-(iii), from left to right, are indicatively separated by dashed gray lines. (a) $\vec{r} = \vec{r}^{(1)}$; (b) $\vec{r} = \vec{r}^{(2)}$. The solid black lines show the predictions of (16) using (14), with $\phi_{i,i+1}$ and $P_{(i,i+1)}$ inferred from simulations. Predictions from (18) are shown as solid colored line. $\widetilde{\phi}_i$ can display a non-monotonic dependence on sK across regimes (ii)-(iii), see text. (c) Chart summarizing the outcome of Stage 1, Stage 2 and the overall fixation probability $\widetilde{\phi}_i$ as function of sK in regimes (i)-(iii), from left to right. In all panels: $\vec{x}_0 = \vec{x}_c$ and $\epsilon = 0$.

need to consider that, after reaching the edge $(i-1,i)$ with a probability $\phi_{i-1,i}$, species i has a probability $1-\phi_{i-1}$ to win against $i-1$ (strong opponent), which yields $\phi_{i-1,i}(1-\phi_{i-1})$. With these two contributions, we obtain

$$\widetilde{\phi}_i = \phi_{i,i+1}\phi_i + \phi_{i-1,i}(1-\phi_{i-1}), \tag{16}$$

which is also a function of sK, see Fig. 4 (a,b). Of particular interest is the situation where the selection intensity is weak, $s \ll 1$, in which case (16) can be simplified by noting $\phi_{i,i+1} \approx \phi_{i-1,i} \simeq 1/3$ and using the result $\phi_i \simeq \phi_i|_K$, given by (15), for the absorption probability in the MCLV with $N = K$, see Sec. S1.2, yielding

$$\widetilde{\phi}_i \simeq \frac{1}{3}\left(1+\phi_i-\phi_{i-1}\right) \approx \frac{1}{3}\left(1+\phi_i|_K-\phi_{i-1}|_K\right). \tag{17}$$

Using the properties of the survival and absorption probabilities $\phi_{i,j}$ and ϕ_j discussed above, we can infer those of $\widetilde{\phi}_i$ in the regimes (i)-(iii):

- Regime (i): At quasi-neutrality, all species have the same this fixation probability to first order: $\widetilde{\phi}_i = 1/3 + O(sK)$. An estimate of the subleading correction is obtained by noticing $\phi_i|_K \simeq \frac{1}{2}(1+\alpha_i K/6)$ when $\alpha_i K \ll 1$. This, together with Eq. (17), gives

$$\widetilde{\phi}_i \simeq \frac{1}{3}\left(1+\frac{sK}{12}(r_i-r_{i-1})\right). \tag{18}$$

This result allows us to understand which are the species (slightly) favored by selection: When $r_1 < r_2, r_3$, Eq. (18) predicts that $\widetilde{\phi}_1$ is less than $1/3$ and decreases with sK, while $\widetilde{\phi}_2 > 1/3$ and increases with sK, and $\widetilde{\phi}_3 = 1/3 + O(s^2)$. These predictions agree with the simulation results of Fig. 4 (a) in regime (i).

- Regime (iii): Under strong selection, the total fixation probability obeys the LOW, as in the cCLV (see Sec. S2). The species overall fixation probabilities are therefore ordered as follows, see Eqs. (S18, S19):

$$\begin{aligned} &\widetilde{\phi}_i > \widetilde{\phi}_{i+1}, \widetilde{\phi}_{i-1} \quad \text{if} \quad r_i < r_{i\pm1}, \quad \text{and} \\ &\widetilde{\phi}_i \approx \widetilde{\phi}_{i+1} > \widetilde{\phi}_{i-1} \quad \text{if} \quad r_i = r_{i+1} < r_{i-1}, \end{aligned} \tag{19}$$

with $\widetilde{\phi}_i \approx \phi_{i,i+1} \overset{sK\gg1}{\longrightarrow} 1$, $1/2$ or 0. These predictions agree with the simulations results of Fig. 4 (a,b).

- Regime (ii): Under weak selection, $\widetilde{\phi}_i$ can vary non-monotonically with sK, see Fig. 4 (a,b). This behavior can be understood by noticing that near the boundary of regimes (i)-(ii), we have $\phi_i \approx 1/3$ that increases with sK if $r_i > r_{i-1}$ and decreases when $r_i < r_{i-1}$, see Eq. (18) and Fig. 4 (a,b). As sK approaches the boundary of regimes (ii)-(iii), the dynamics is increasingly governed by the LOW with $\widetilde{\phi}_i \approx \phi_{i,i+1} \overset{sK\gg1}{\longrightarrow} 1$, $1/2$ or 0. This can lead to a non-monotonic dependence on sK: For instance, if $r_1 < r_2, r_3$, $\widetilde{\phi}_1$ decreases and $\widetilde{\phi}_2$ increases about the value $1/3$ near the (i)-(ii) boundary, and then respectively increases and decreases as sK approaches the boundary (ii)-(iii), and through regime (iii) where $\widetilde{\phi}_1 \to 1$ while $\widetilde{\phi}_2 \to 0$, see Fig. 4 (a).

The main features of the survival, absorption and overall fixation probabilities in the constant-K BDCLV are summarized in the chart of Fig. 4 (c).

3.2. Mean fixation time in the constant-K BDCLV

The overall mean fixation time T_F is the average time after which one of the species takes over the entire population. This quantity consists of one contribution arising from Stage 1, referred to as the *mean extinction time* T_1, and the *mean absorption time* T_2 arising from Stage 2. In Sec. S5.1, we study T_1 and T_2 in the regimes (i)-(iii) and show that, when $\vec{x}_0 = \vec{x}_c$, the overall mean fixation time $T_F = T_1 + T_2 = O(K)$, see Fig. S4 (c). Since $N(t) \simeq K$ after a short transient, this means that species coexistence is lost after a mean time scaling linearly with the population size. We also show that T_1 and T_2 are both of order $O(K)$ in regimes (i)-(ii) and $T_1 \gg T_2$ in the regime (iii), see Figs. S4 (a,b) and 1.

4. CLV with randomly switching carrying capacity

In many biological applications, the population is subject to sudden and extreme environmental changes dramatically affecting its size [60, 59, 52, 53, 54]. The variation of $N(t)$ leads to a coupling between demographic fluctuations which greatly influence the population's evolution [56, 57, 52, 53, 54].

Here, we study the *coupled* effect of demographic and environmental fluctuations on the BDCLV fixation properties by considering the randomly-switching carrying capacity (4), modeled in terms of the stationary dichotomous noise (3), that can also be written as

$$K(t) = \langle K\rangle(1+\gamma\xi(t)), \quad \text{with } \gamma \equiv \frac{K_+ - K_-}{2\langle K\rangle}$$

where $0 < \gamma < 1$ is a parameter measuring the intensity of the environmental variability. In fact, the variance of $K(t)$ is $\mathrm{var}(K(t)) = (\gamma\langle K\rangle)^2$, and we can write $K_\pm = (1\pm\gamma)\langle K\rangle$. In order to study the influence of environmental variability on the population dynamics, we consider $\gamma = O(1)$ and $\langle K\rangle \gg 1$. This ensures that the population is subject to significant environmental variability ($\mathrm{var}(K) \gg 1$), and its typical size is large enough to avoid that demographic fluctuations alone are the main source of randomness. In all our simulations, the initial value of $K(t)$ is either K_+ or K_- with probability $1/2$.

From the master equation (7), proceeding as in Sec. S1.1, the population composition is found to still evolve according to Eqs. (9) when all demographic fluctuations are neglected. However, now the random switching of $K(t)$ drives the stochastic evolution of the population size which, when demographic noise is ignored, obeys $\dot{N} = N(1 - N/K_{\pm})$ if $\xi = \pm 1$, see Eq. (S8). This can be rewritten as

$$\dot{N} = N\left(1 - \frac{N}{\mathcal{K}}\{1 - \gamma\xi(t)\}\right), \tag{20}$$

where

$$\mathcal{K} \equiv (1 - \gamma^2)\langle K\rangle = \frac{2K_+K_-}{K_+ + K_-}$$

is the harmonic mean of $K_\pm$ and ξ is the multiplicative dichotomous noise (3). The external noise intensity being $N^2\gamma/\mathcal{K}$, the environmental fluctuations increase with γ together with $\mathrm{var}(K) = (\gamma\langle K\rangle)^2$. Eq. (20) defines a piecewise-deterministic Markov process [66]. When $\nu \to \infty$, the environmental noise self averages, with $\xi \to \langle\xi\rangle = 0$ in (20) which reduces to the logistic equation (8) with a renormalized carrying capacity $K \to \mathcal{K}$ [56, 57]. Again, a timescale separation arises when $s \ll 1$, with N evolving faster than x_i's: N settles in its quasi-stationary distribution (N-QSD) in a time $t = O(1)$, while the x_i's change on a timescale $t = O(1/s)$, see Fig. 1 (c).

The process defined by Eq. (20) [63, 64, 43, 56, 57] is characterized by the following stationary marginal probability density function (pdf) [56]:

$$p_\nu^*(N) = \frac{\mathcal{Z}}{N^2}\left[\frac{(K_+ - N)(N - K_-)}{N^2}\right]^{\nu-1}, \tag{21}$$

where $\mathcal{Z}$ is the normalization constant. The pdf p_ν^* gives the long-time probability density of N on the support $N \in [K_-, K_+]$ regardless of the environmental state ξ [63, 64]. When $\gamma = O(1)$ and $\langle K\rangle \gg 1$, p_ν^* is a good approximation of the N-QSD even if it ignores the effect of the IN, see Fig. 5. In fact, the comparison of p_ν^* and N-QSD shown in Fig. 5 reveals that p_ν^* correctly captures the main features of the N-QSD, such as the location of the peak(s) and its right-tailed skewness, whereas it fails to capture the width about the peak(s) [3]. However, for our purposes here the process defined by (20) is sufficient to characterize the system's fixation properties [56, 57]. It is noteworthy that p_ν^* and the N-QSD are bimodal if $\nu < 1$, with peaks at $N \simeq K_\pm$, see Fig. 5 (a,b). When $\nu > 1$, p_ν^* and N-QSD are unimodal and N fluctuates about the maximum of p_ν^* given by $N^* = \langle K\rangle(1+\nu)\left(1 - \sqrt{1 - 4\nu(1-\gamma^2)/(1+\nu)^2}\right)/2$. The value of N^* increases with ν at γ fixed, see Fig. 5 (c,d), and decreases with γ (environmental variability) at ν fixed. When $\nu \to \infty$, we have $N^* \to \mathcal{K}$ and p_ν^* is sharply peaked about $\mathcal{K}$, as expected from the self-averaging of $\xi(t)$ when $\nu \gg 1$, see Fig. 5 (d). In this case, we recover the constant-K BDCLV dynamics with $K \to \mathcal{K}$.

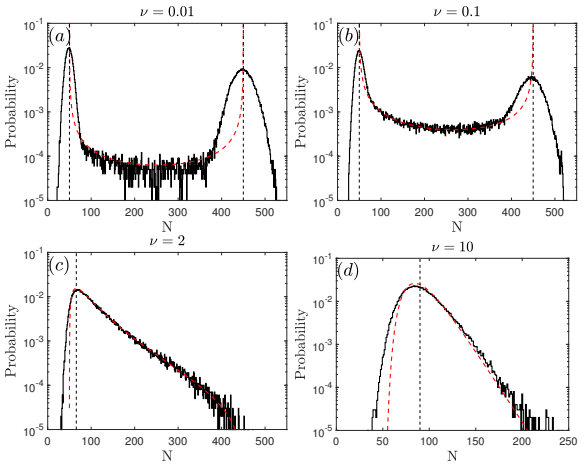

Figure 5: N-QSD and $p_\nu^*(N)$ for (a) $\nu = 0.01$, (b) $\nu = 0.1$, (c) $\nu = 2$, (d) $\nu = 10$. Parameters are $(s, K_+, K_-) = (0.02, 450, 50)$. Solid lines are histograms from stochastic simulations and colored dashed lines are predictions from (21), see text. Black dashed lines indicate $N = K_\pm$ in (a) and (b), $N = N^*$ in (c), and $N = \mathcal{K}$ in (d), see text.

4.1. *Survival, absorption and fixation probabilities in the switching-K BDCLV*

As in the constant-K BDCLV, the total fixation probability $\widetilde{\phi}_i$ depends on the stage 1 survival and stage 2 absorption probabilities. Here, we analyze the effect of the environmental randomness on these quantities, by distinguishing again the regimes of (i) quasi-neutrality, where $s \ll 1$ and $s\langle K\rangle \ll 1$; (ii) weak selection, where $s \ll 1$ and $s\langle K\rangle = O(10)$; and (iii) strong selection, where $s = O(1)$ and $sK \gg 1$.

4.1.1. *Stage 1: Survival probabilities in the switching-K BDCLV*

To analyze the survival probability $\phi_{i,i+1}$ in the switching-K BDCLV, it is convenient to consider this quantity in the limits $\nu \to \infty$ and $\nu \to 0$, where $\phi_{i,i+1}$ can be expressed in terms of $\phi_{i,i+1}|_K$, the survival probability in the constant-K BDCLV studied in Sec. 3.1.1.

[3] This stems from the demographic fluctuations being ignored by the process defined by (20): These cause a "leakage" of the distribution of N outside $[K_-, K_+]$. This is particularly visible when $\nu < 1$, see Fig. 5 (a). As shown in Ref. [57], the actual width of the N-QSD can be accurately computed with a linear-noise approximation about the process defined by (20).

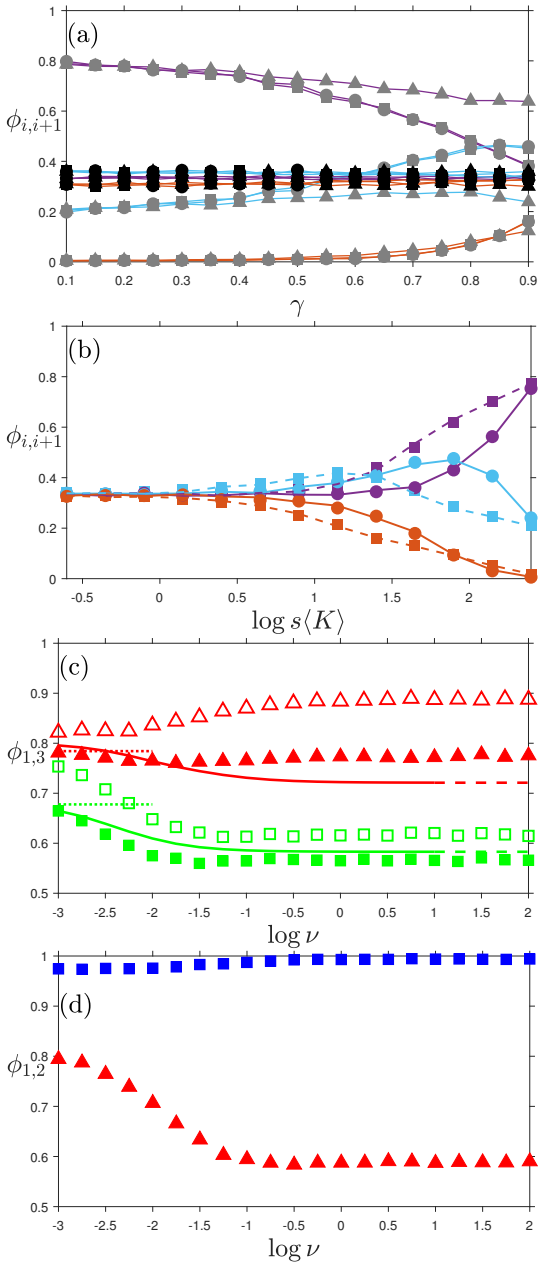

Figure 6: (a) Stage 1 survival probability $\phi_{i,i+1}$ vs. γ for $\langle K\rangle = 250$ kept fixed ($K_+ \in [275, 475]$ and $K_- \in [25, 225]$). and $s = 0.01$ (black), $s = 0.4$ (gray). Simulation results for $\nu = 10$ (circles), $\nu = 1.2$ (squares) and $\nu = 0.001$ (triangles). (b) $\phi_{i,i+1}$ vs. $s\langle K\rangle$ for $\langle K\rangle = 250, \gamma = 0.8$ and $s \in \{10^{-k/4}, k = 0, \ldots, 12\}$ kept fixed, with $\nu = 2$ (circles) and $\nu = 0.001$ (squares); lines are $\phi_{i,j}|_{(1-\gamma^2)\langle K\rangle}$ (solid) and $\frac{1}{2}(\phi_{i,j}|_{(1+\gamma)\langle K\rangle} + \phi_{i,j}|_{(1-\gamma)\langle K\rangle})$ (dashed) are from the constant-$\langle K\rangle$ BDCLV. In panels (a,b) $\vec{r} = \vec{r}^{(1)}$, $\phi_{1,2}$ in purple, $\phi_{2,3}$ in light blue, $\phi_{3,1}$ in orange. (c) Stage 2 absorption probabilities ϕ_1 (red triangles) and ϕ_3 (green squares) vs. ν for $\langle K\rangle = 250$ and $\gamma = 0.8$ kept fixed and $\vec{r} = \vec{r}^{(2)}$. Symbols are from simulations with $s = 0.1$ (open) and $s = 10^{-5/4} \approx 0.056$ (filled). Lines are from (26) (solid), (25) (dashed), (24) (dotted), and assume $P_{i,i+1} \approx 1$; they capture reasonably well the ν-dependence of ϕ_1 and ϕ_3 when $s\langle K\rangle \lesssim 10$, see text. (d) Same as in panel (c) for ϕ_1 (red triangles) and ϕ_2 (blue squares) vs. ν with $s = 10^{-1/4}$ and $\vec{r} = \vec{r}^{(1)}$. In all panels $\vec{x}_0 = \vec{x}_c$, $\epsilon = 0$.

When $\nu \to \infty$, many switches occur in Stage 1 and the dichotomous noise self averages, $\xi \to \langle\xi\rangle = 0$ [56, 57]. The population thus rapidly settles in its N-QSD that is delta-distributed at $N = (1-\gamma^2)\langle K\rangle$ when $\langle K\rangle \gg 1$. Hence, the stage 1 dynamics under fast switching is similar to the cCLV dynamics in a population of size $(1-\gamma^2)s\langle K\rangle$, see Sec. S2. This yields $\phi_{i,i+1} \overset{\nu\to\infty}{=} \phi_{i,i+1}|_{(1-\gamma^2)\langle K\rangle}$.

When $\nu \to 0$, there are no switches in Stage 1, and the extinction of the first species is equally likely to occur in each environmental state $\xi = \pm 1$ (with $K = (1\pm\gamma)\langle K\rangle$). This gives $\phi_{i,i+1} \overset{\nu\to 0}{=} \left(\phi_{i,i+1}|_{(1+\gamma)\langle K\rangle} + \phi_{i,i+1}|_{(1-\gamma)\langle K\rangle}\right)/2$.

The case of intermediate ν can be inferred from the above by noting that the average number of switches occurring in Stage 1 is $O(\nu\langle K\rangle)$, see Fig. S6 (a). As the population experiences a large number of switches in Stage 1 when $\nu = O(1)$ and $\langle K\rangle \gg 1$, the dichotomous noise effectively self-averages, $\xi(t) \simeq \langle\xi\rangle = 0$, and therefore

$$\phi_{i,i+1} \overset{\nu=O(1)}{\approx} \phi_{i,i+1}|_{(1-\gamma^2)\langle K\rangle}. \tag{22}$$

When $\nu \ll 1/\langle K\rangle$, there are very few or no switches after a time of order $O(\langle K\rangle)$ prior to extinction the first species, and therefore

$$\phi_{i,i+1} \overset{\nu\ll 1/\langle K\rangle}{\approx} \frac{1}{2}\left(\phi_{i,i+1}|_{(1+\gamma)\langle K\rangle} + \phi_{i,i+1}|_{(1-\gamma)\langle K\rangle}\right). \tag{23}$$

Eq. (22) implies that for any $\nu = O(1)$, the survival probability of species $i, i+1$, i.e the probability that species $i-1$ dies out first, is given by the survival probability in the constant-K BDCLV with $K = \langle K\rangle$ (same average carrying capacity) and a rescaled selection intensity $(1-\gamma^2)s$. The effect of random switching is therefore to effectively reduce the selection intensity by a factor $1-\gamma^2 = 1 - (\mathrm{var}(K(t))/\langle K\rangle^2)$ proportional to the variance of the carrying capacity. The $s\langle K\rangle$-dependence of $\phi_{i,i+1}$ can thus readily be obtained from Fig. 3 (a,b) by rescaling $s \to (1-\gamma^2)s$ as shown in Fig. 6 (a,b). Hence, when there is enough environmental variability (γ large enough) the survival scenarios differ from those of the constant-K BDCLV and depend on the switching rate:

- When $\nu \gg 1/\langle K\rangle$, switching reduces the selection by a factor $1-\gamma^2$, see Fig. 6 (b). Hence, there is a critical γ^*, estimated as $\gamma^* \approx (1 - 50/s\langle K\rangle)^{1/2}$, such that $\phi_{i,i+1}$ obeys the LOSO when $\gamma > \gamma^*$ and $s\langle K\rangle \gg 1$, while the LOW still applies when $\gamma < \gamma^*$. Therefore, when $\gamma > \gamma^*$, all species have a finite chance to survive Stage 1, with probabilities ordered according to the LOSO, ($\phi_{1,2} \approx \phi_{2,3} > \phi_{3,1}$ with $\gamma^* \approx 0.7$, in Fig. 6 (a)). Fig. 6 (a), also shows that the exact value ν has little influence on $\phi_{i,i+1}$ provided that $\nu\langle K\rangle \gg 1$ (circles and

squares almost coincide).

- When $\nu \ll 1/\langle K\rangle$, we have $\phi_{i,i+1} \approx (\phi_{i,i+1}|_{K_+} + \phi_{i,i+1}|_{K_-})/2$. Hence, if $s\langle K\rangle \gg 1$ and $\gamma > \hat{\gamma}$, where $\hat{\gamma} \approx 1 - 50/s\langle K\rangle$, $\phi_{i,i+1}|_{K_+}$ follows the LOW whereas $\phi_{i,i+1}|_{K_-}$ obeys the LOSO, and the $\phi_{i,i+1}$'s therefore interpolate between LOW and LOSO values: For $\gamma > \hat{\gamma}$, the survival probabilities under strong selection and slow switching deviate markedly from the purely LOW values of $\phi_{i,i+1}|_{\langle K\rangle}$ which asymptotically approach 0, 1 or 1/2 (see triangles in Fig. 6 (a) where $\hat{\gamma} \approx 0.5$).

When $s \ll 1$ and $s\langle K\rangle = O(10)$ in regime (ii), changing γ has little effect on the survival probabilities: the survival probabilities $\phi_{i,i+1} \approx 1/3$, and remain ordered according to the LOSO (see black symbols in Fig. 6 (a)).

These results show that environmental variability leads to new survival scenarios in the BDCLV under strong selection: When there is enough variability, all species have a finite probability to survive even when $s\langle K\rangle \gg 1$. The departure from the pure LOW survival scenario is most marked in the generic case of a finite switching rate ($\nu \gg 1/\langle K\rangle$). With respect to the constant-K BDCLV, the general effect of random switching in Stage 1 is therefore to "level the field" by hindering the onset of the zero-one LOW. Since BDCLV survival probability $\phi_{i,i+1}$ coincides with the fixation probability of species i in the cCLV, see Sec. S2, it is noteworthy that these results also show that random switching can lead to new survival/fixation scenarios in the cCLV when the variance of the carrying capacity is sufficiently high.

4.1.2. Stage 2: Absorption probabilities in the switching-K BDCLV

Stage 2 consists of the competition between types i and $i+1$ along the edge $(i, i+1)$ of S_3. This starts with an initial fraction $\hat{x}_i$ of i individuals and ends up with the absorption of one of the species with probabilities ϕ_i (for species i) and $1-\phi_i$ (for $i+1$). Again $\hat{x}_i$ is randomly distributed according to a probability density $P_{(i,i+1)}$ resulting from Stage 1, see Sec. S4 [4]. Since $\phi_i \approx 1/2$ at quasi-neutrality and $\phi_i \approx 1$ under strong selection, see Fig. 6 (c,d), Stage 2 dynamics is nontrivial in regime (ii). To analyze the stage 2 dynamics under weak selection $s \ll 1$ and $\langle K\rangle \gg 1$, it is again useful to consider the limits $\nu \to 0$ and $\nu \to \infty$:

[4] The probability density function of $\hat{x}_i$ is generally different in the constant-K and switching-K BDCLV, see Fig. S3. Yet, for the sake of simplicity, with a slight abuse of notation, we denote these two quantities by $P_{i,i+1}(\hat{x}_i)$.

- When $\nu \to 0$, there are no switches in Stage 2 and absorption is equally likely to occur in the static environment $K = K_-$ or $K = K_+$. Hence, if the fraction $\hat{x}_i$ is known, we have $\phi_i(\hat{x}_i) \overset{\nu\to 0}{=} \phi_i^{(0)}(\hat{x}_i) = \frac{1}{2}\left(\phi_i(\hat{x}_i)|_{K_-} + \phi_i(\hat{x}_i)|_{K_+}\right)$, where $\phi_i(\hat{x}_i)|_K = (1 - e^{-\alpha_i K\hat{x}_i})/(1 - e^{-\alpha_i K})$, see (13). Since $\hat{x}_i$ is randomly distributed, one needs to integrate over $P_{(i,i+1)}$: $\phi_i \overset{\nu\to 0}{\equiv} \phi_i^{(0)} = \int_0^1 \phi_i^{(0)}(\hat{x}_i) P_{(i,i+1)}(\hat{x}_i)\, d\hat{x}_i$. In general, $P_{(i,i+1)}$ is obtained from stochastic simulations and has been found to be mostly independent of ν, see Fig. S3 (c,d). When $s \ll 1$ with $s\langle K\rangle \lesssim 10$, we can again assume $P_{(i,i+1)} \approx 1$ (uniform distribution), which allows us to obtain

$$\phi_i \overset{\nu\to 0}{=} \phi_i^{(0)} \simeq \frac{1}{2}\left(\phi_i|_{K_-} + \phi_i|_{K_+}\right), \quad \text{where} \tag{24}$$

$\phi_i|_K \equiv (e^{-\alpha_i K} + \alpha_i K - 1)/(\alpha_i K(1 - e^{-\alpha_i K}))$, see (15).

- When $\nu \to \infty$, the environmental noise self averages ($\xi \to \langle\xi\rangle = 0$) [56, 57], and the absorption occurs subject to the effective $K(t) = \mathcal{K}$, see Eq. (20). Hence, when $\hat{x}_i$ is known, $\phi_i(\hat{x}_i) \overset{\nu\to\infty}{=} \phi_i^{(\infty)}(\hat{x}_i) = \phi_i(\hat{x}_i)|_{\mathcal{K}}$, whose integration over $P_{(i,i+1)}$ gives the absorption probability: $\phi_i \overset{\nu\to\infty}{\equiv} \phi_i^{(\infty)} = \int_0^1 \phi_i^{(\infty)}(\hat{x}_i)\, P_{(i,i+1)}(\hat{x}_i)\, d\hat{x}_i$. When $s \ll 1$ with $s\langle K\rangle \lesssim 10$, and $P_{(i,i+1)} \approx 1$, we have

$$\phi_i \overset{\nu\to\infty}{=} \phi_i^{(\infty)} \simeq \phi_i|_{\mathcal{K}} = \frac{e^{-\alpha_i\mathcal{K}} + \alpha_i\mathcal{K} - 1}{\alpha_i\mathcal{K}(1 - e^{-\alpha_i\mathcal{K}})}. \tag{25}$$

- When the switching rate ν is finite and $s \ll 1$, with $s\langle K\rangle = O(10)$, the probability ϕ_i can be computed as in Ref. [56] by exploiting the time scale separation between N and x_i, and by approximating the N-QSD by the marginal stationary probability density (21). In this framework, ϕ_i can be computed by averaging $\phi_i(\hat{x}_i)|_N = (1 - e^{-\alpha_i N\hat{x}_i})/(1 - e^{-\alpha_i N})$ over the rescaled probability density (21) [56, 57]:

$$\phi_i(\hat{x}_i) \simeq \phi_i^{(\nu)}(\hat{x}_i) = \int_{K_-}^{K_+} \phi_i(\hat{x}_i)|_N\; p^*_{\nu/\alpha_i}(N)\, dN,$$

where p^*_{ν/α_i} is given by (21) with a rescaled switching rate $\nu \to \nu/\alpha_i$ due to an average number $O(\nu/\alpha_i)$ of switches occurring in Stage 2, see [57] and Sec. S5.3. As above, the absorption probability is obtained by formally integrating over $P_{(i,i+1)}$, i.e. $\phi_i \simeq \phi_i^{(\nu)} \equiv \int_0^1 \phi_i^{(\nu)}(\hat{x}_i)\, P_{(i,i+1)}(x_i)\, d\hat{x}_i$. Under weak selection, we can approximate $P_{(i,i+1)} \approx 1$, see Sec. S4, and, using (14) and (15), we obtain

$$\phi_i \simeq \phi_i^{(\nu)} \approx \int_{K_-}^{K_+} \left\{\frac{e^{-N\alpha_i} + \alpha_i N - 1}{\alpha_i N\left(1 - e^{-\alpha_i N}\right)}\right\} p^*_{\nu/\alpha_i}(N)\, dN. \tag{26}$$

The uniform approximation of $P_{(i,i+1)} \approx 1$ is legitimate when $s\langle K\rangle = O(10)$, and has broader range applicability than in the constant-K case, see Sec. S4 and Fig. S3. Hence, Eq. (26), along with (24) and (25), captures the ν-dependence of ϕ_i over a broad range of values ν when $s \ll 1$. In fact, simulation results of Fig. 6 (c,d) show that the ϕ_i's generally have a non-trivial ν-dependence. When $s \ll 1$ and $s\langle K\rangle = O(10)$, this is satisfactorily captured by (24)-(26), with $\phi_i^{(\nu)} \approx \phi_i^{(0)}$ when $\nu \ll 1$, and $\phi_i^{(\nu)} \approx \phi_i^{(\infty)}$ when $\nu \gg 1$, see Fig. 6 (c, filled symbols). Clearly, the assumption $P_{(i,j)} \approx 1$ and the timescale separation break down when $s = O(1)$ [57], and the approximations (24)-(26) are then no longer valid.

4.1.3. *Overall fixation probabilities in the switching-K BDCLV*

The overall fixation probability $\widetilde{\phi}_i$ is obtained from the survival and absorption probabilities according to $\widetilde{\phi}_i = \phi_{i,i+1}\phi_i + \phi_{i-1,i}(1-\phi_{i-1})$, see Eq. (16).

In order to study the influence of the environmental variability on $\widetilde{\phi}_i$, it is again useful to consider the limiting cases of fast/slow switching. In fact, as shown in Fig. 7, when $\nu \to \infty, 0$, the overall fixation probability is given by $\widetilde{\phi}_i \to \widetilde{\phi}_i^{(\infty)}$ when $\nu \to \infty$ and $\widetilde{\phi}_i \to \widetilde{\phi}_i^{(0)}$ when $\nu \to 0$, with

$$\widetilde{\phi}_i^{(\infty)} \equiv \widetilde{\phi}_i|_{\mathcal{K}} = \widetilde{\phi}_i|_{(1-\gamma^2)\langle K\rangle} \tag{27}$$

$$\widetilde{\phi}_i^{(0)} \equiv \frac{1}{2}\left(\widetilde{\phi}_i|_{(1+\gamma)\langle K\rangle} + \widetilde{\phi}_i|_{(1-\gamma)\langle K\rangle}\right), \tag{28}$$

where $\widetilde{\phi}_i|_K$ is the overall fixation probability in the BDCLV with constant carrying capacity K, see Fig. 4 (a,b). These results stem from the outcomes of Stage 2 when $s\langle K\rangle \ll 1$ and from Stage 1 when $s\langle K\rangle \gg 1$:

- When $s\langle K\rangle \ll 1$, in regime (i) and about the boundary of regimes (i)-(ii): $\phi_{i,i+1} \approx 1/3$ for all species and $P_{(i,i+1)} \approx 1$, see Sec. S4. The overall fixation probabilities are thus given by $\widetilde{\phi}_i \approx (1 + \phi_i - \phi_{i-1})/3$, where $\phi_i \approx \phi_i^{(\infty)}$ if $\nu/s \gg 1$ and $\phi_i \approx \phi_i^{(0)}$ if $\nu/s \ll 1$, yielding (to leading order in $s\langle K\rangle$)

$$\widetilde{\phi}_i \approx \widetilde{\phi}_i|_\kappa = \frac{1}{3}\left[1 + \frac{s\kappa}{12}(r_i - r_{i-1})\right], \tag{29}$$

where $\kappa = (1-\gamma^2)\langle K\rangle$ if $\nu/s \gg 1$ and $\kappa = \langle K\rangle$ if $\nu/s \ll 1$. In agreement with Fig. 7, Eq. (29) predicts that $\widetilde{\phi}_i$ is greater than $1/3$ and increases with $s\langle K\rangle$ (at ν fixed) if $r_i > r_{i-1}$, whereas $\widetilde{\phi}_i$ is less than $1/3$ and is a decreasing function of $s\langle K\rangle$ (at ν constant) when $r_i < r_{i-1}$.

- When $\alpha_i\langle K\rangle \gg 1$, about the boundary of regimes (ii)-(iii) and in regime (iii): Selection strongly favors species i on edge $(i, i+1)$ in Stage 2, and the fixation probability is determined by the outcome of Stage 1: $\widetilde{\phi}_i \approx \widetilde{\phi}_i^{(\infty)}$ if $\nu \gg 1/\langle K\rangle$ and $\widetilde{\phi}_i \approx \widetilde{\phi}_i^{(0)}$ when $\nu \ll 1/\langle K\rangle$.

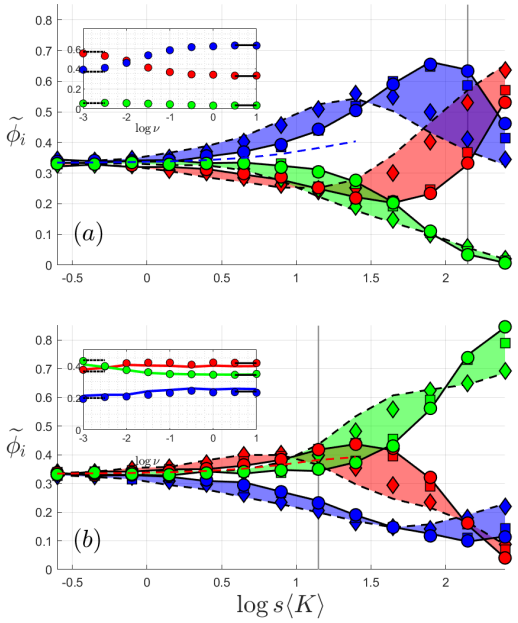

Figure 7: Total fixation probabilities $\widetilde{\phi}_i$ vs. $s\langle K\rangle$ for values of $s \in (10^{-3}, 1)$ and with $\langle K\rangle = 250$ and $\gamma = 0.8$ kept fixed, see text. (a) $\vec{r} = \vec{r}^{(1)}$; (b) $\vec{r} = \vec{r}^{(2)}$. Shaded areas and symbols are from stochastic simulations with $\nu = 10$ (○), $\nu = 0.1$ (□), $\nu = 10^{-5/2}$ (◇). Solid and dashed black lines show respectively $\widetilde{\phi}_i|_{\mathcal{K}}$ and $(\widetilde{\phi}_i|_{K_-} + \widetilde{\phi}_i|_{K_+})/2$ in both panels and insets, see text. Vertical light gray lines indicate $\widetilde{\phi}_i$ for $s = 10^{-1/4}$ (a) and $s = 10^{-5/4}$ (b). $\widetilde{\phi}_i$ increases with ν when the solid black line is above the dashed black line, otherwise $\widetilde{\phi}_i$ decreases with ν, see text. Dashed colored lines show $\widetilde{\phi}_2$ in (a) and $\widetilde{\phi}_1$ in (b) obtained from $\widetilde{\phi}_i \approx (1 + \phi_i - \phi_{i-1})/3$, with (26) and $\nu = 10$. Insets: $\widetilde{\phi}_i$ vs. ν for $s = 10^{-1/4}$ (a) and $s = 10^{-5/4}$ (b); symbols are from stochastic simulations and solid lines in inset (b) are predictions of (16) obtained using (26), with $\phi_{i,i+1}, \phi_{i-1,i}$ inferred from simulations. Fixation scenario changes at $\nu = \nu^*(s)$ with $\nu^* \approx 10^{-2}$ in (a) and $\nu^* \approx 10^{-5/2}$ in (b), see text. In all panels and insets: species 1 in red, species 2 in blue, species 3 in green; $\vec{x}_0 = \vec{x}_c$, $\epsilon = 0$.

Hence, in regime (i) and about the boundary of regimes (i)-(ii) and (ii)-(iii), as well as in regime (iii) we have $\widetilde{\phi}_i \to \widetilde{\phi}_i^{(\infty)}$ when $\nu \to \infty$ and $\widetilde{\phi}_i \to \widetilde{\phi}_i^{(0)}$ when $\nu \to 0$. We have found that the fixation probabilities of the species surviving Stage 1 vary monotonically with ν, whereas the fixation probability of the species most likely to die out first varies little with ν, see the insets of Fig. 7. Therefore, as corroborated by Fig. 7, for finite switching rates, we have

$$\min\left(\widetilde{\phi}_i^{(0)}, \widetilde{\phi}_i^{(\infty)}\right) < \widetilde{\phi}_i < \max\left(\widetilde{\phi}_i^{(0)}, \widetilde{\phi}_i^{(\infty)}\right). \tag{30}$$

Taking into account the average number of switches arising in Stages 1 and 2, see Sec. S5.3, we have $\widetilde{\phi}_i \approx \widetilde{\phi}_i^{(\infty)}$ when $\nu \gg \max(s, 1/\langle K\rangle)$ and $\widetilde{\phi}_i \approx \widetilde{\phi}_i^{(0)}$ if

$\nu \ll \min(s, 1/\langle K\rangle)$, see Fig. 7.

According to Eqs. (27)-(30), the fixation probabilities under random switching can be inferred from $\widetilde{\phi}_i|_K$ obtained in the constant-K BDCLV with a suitable value of K:
- Under fast switching, $\widetilde{\phi}_i$ coincides with $\widetilde{\phi}_i|_{(1-\gamma^2)\langle K\rangle}$. Since $\widetilde{\phi}_i|_K$ is a function of sK, when the average carrying capacity $\langle K\rangle$ is kept fixed, $\widetilde{\phi}$ is thus given by $\widetilde{\phi}_i|_{\langle K\rangle}$ subject to a rescaled selection intensity $(1-\gamma^2)s$. Hence, when $\nu \gg \max(s, 1/\langle K\rangle)$ and $\langle K\rangle$ is kept fixed, the effect of random switching is to reduce the selection intensity by a factor $1 - \mathrm{var}(K(t))/\langle K\rangle^2$.
- Under slow switching, $\widetilde{\phi}_i$ is given by the arithmetic average of $\widetilde{\phi}_i|_{K_+}$ and $\widetilde{\phi}_i|_{K_-}$. When the average carrying capacity $\langle K\rangle$ is kept fixed, $\widetilde{\phi}$ is thus given by the average of $\widetilde{\phi}|_{\langle K\rangle}$ subject to a selection intensity $(1 + \gamma)s$ and $(1 - \gamma)s$. These predictions, agree with the results of Fig. 7, and imply that the $s\langle K\rangle$-dependence of $\widetilde{\phi}_i$ can be readily obtained from Fig. 4 (a,b).

At this point, we can discuss the effect of random switching on $\widetilde{\phi}_i$ by comparison with $\widetilde{\phi}_i|_{\langle K\rangle}$ in the constant-K BDCLV, when $\langle K\rangle$ is kept fixed:

- *Random switching "levels the field" of competition and balances the effect of selection*: The species that is the least likely to fixate has a higher fixation probability under random switching than under a constant $K = \langle K\rangle$, compare Figs. 4 (a,b) and 7 (see also Fig. 8): Dichotomous noise balances the selection pressure that favors the fixation of the other species, and hence levels the competition.

- *Random switching effectively reduces the selection intensity under fast switching*: When $\nu \gg \max(s, 1/\langle K\rangle)$, we have seen $\widetilde{\phi}_i = \widetilde{\phi}_i|_{\langle K\rangle}$ subject to a rescaled selection intensity $(1 - \gamma^2)s = (1 - \mathrm{var}(K(t))/\langle K\rangle^2)s$. Fast random switching therefore reduces the selection intensity proportionally to the variance of K. Hence, under strong selection and fast switching, a zero-one LOW appears in the switching-K BDCLV only in a population whose average size is $1/(1 - \gamma^2)$ times greater than in the constant-K BDCLV. This means that when K has a large variance (large γ) the onset of the zero-one LOW, with $\widetilde{\phi}_i \to 0, 1/2, 1$, in the fast switching-$K$ BDCLV arises when $s\langle K\rangle \gg 1$ and $\langle K\rangle$ is at least one order of magnitude larger than in the constant-K BDCLV (*e.g.*, $\langle K\rangle \gtrsim 10^4$ instead of $\langle K\rangle \gtrsim 10^3$ when $\gamma = 0.8$), see also Fig. 8.

- *Random switching can yield new fixation scenarios*: Which species is the most likely to fixate can vary with ν and γ, at s and $\langle K\rangle$ fixed, and does not generally obey a simple law (neither LOW nor LOSO). When the environmental variance is large enough ($\gamma \gtrsim \gamma^*$) the shaded areas of Fig. 7 can overlap. This occurs when the fixation probabilities of the two most likely species to prevail cross, see insets of Fig. 7. This yields different fixation scenarios below/above a critical switching rate $\nu^*(s)$: one of these species is the best off at low switching rate, while the other is the best to fare under fast switching. These crossings therefore signal a stark departure from the LOW/LOSO laws. For a crossing between $\widetilde{\phi}_i$ and $\widetilde{\phi}_{i+1}$ to be possible, one, say $\widetilde{\phi}_i$, should decrease and the other increase with ν, i.e. $\widetilde{\phi}_i^{(\infty)} < \widetilde{\phi}_i^{(0)}$ and $\widetilde{\phi}_{i+1}^{(\infty)} > \widetilde{\phi}_{i+1}^{(0)}$ Thus, if $\widetilde{\phi}_i^{(0)} > \widetilde{\phi}_{i+1}^{(0)}$ and $\widetilde{\phi}_i^{(\infty)} < \widetilde{\phi}_{i+1}^{(\infty)}$, there is a critical switching rate $\nu = \nu^*(s)$ where $\widetilde{\phi}_i = \widetilde{\phi}_{i+1}$. The crossing conditions can be determined using (27) and (28). A new fixation scenario emerges when the switching rate varies across ν^*: $\widetilde{\phi}_{i+1} > \widetilde{\phi}_i$ when $\nu > \nu^*$, while $\widetilde{\phi}_{i+1} \leq \widetilde{\phi}_i$ when $\nu \leq \nu^*$. Intuitively, crossings are possible when the variance of K is large ($\gamma \gtrsim \gamma^*$), ensuring that Stage 1 ends up with comparable probabilities of hitting two edges of S_3, and when the two most likely species to fixate have a different ν-dependence arising from Stage 2, see Fig. 6 (c,d). In the inset of Fig. 7 (a), $\widetilde{\phi}_1$ decreases and $\widetilde{\phi}_2$ increases with ν; they intersect at $\nu = \nu^* \approx 0.01$ for $s = 10^{-1/4}$: Species 1 is the most likely to fixate at $\nu < \nu^*$ and species 2 the most likely to prevail at $\nu > \nu^*$, and we have $\widetilde{\phi}_1 > \widetilde{\phi}_2 \gg \widetilde{\phi}_3$ for $\nu < \nu^*$ and $\widetilde{\phi}_2 \gg \widetilde{\phi}_1 > \widetilde{\phi}_3$ when $\nu > \nu^*$. This is to be contrasted with Fig. 4 (a), where the LOW yields $\widetilde{\phi}_1|_{\langle K\rangle} \gg \widetilde{\phi}_2|_{\langle K\rangle} \gg \widetilde{\phi}_3|_{\langle K\rangle}$. The inset of Fig. 7 (b), shows another example of a fixation scenario that depends on ν, with $\widetilde{\phi}_3 > \widetilde{\phi}_1 > \widetilde{\phi}_2$ when $\nu < \nu^* \approx 0.003$ and $\widetilde{\phi}_1 > \widetilde{\phi}_3 > \widetilde{\phi}_2$ when $\nu > \nu^*$.

The main effect of the random switching of K is therefore to balance the influence of selection and to "level the field" of cyclic dominance according to (27)-(30). This is particularly important under strong selection and large K variability, when random switching hinders the LOW by effectively promoting the fixation of the species that are less likely to prevail under constant $K = \langle K\rangle$. This can result in new fixation scenarios in which the most likely species to win varies with the variance and rate of change of the carrying capacity. The CLV fixation scenarios are therefore richer and more complex when demographic and environmental noise are coupled than when they are independent of each other as, *e.g.*, in Ref. [33].

To rationalize further how environmental variability

affects the fixation probabilities, we compute the ratio

$$\rho_i \equiv \frac{\widetilde{\phi}_i}{\widetilde{\phi}_i|_{\langle K\rangle}}. \tag{31}$$

Using (27) and (28), we have $\rho_i \to \rho_i^{(\infty)} \equiv \widetilde{\phi}_i|_{(1-\gamma^2)\langle K\rangle}/\widetilde{\phi}_i|_{\langle K\rangle}$ and $\rho_i \to \rho_i^{(0)} \equiv (\widetilde{\phi}_i|_{K_-} + \widetilde{\phi}_i|_{K_+})/(2\widetilde{\phi}_i|_{\langle K\rangle})$ for fast and slow switching, respectively. We say that random switching enhances the fixation of species i when $\rho_i > 1$, whereas dichotomous noise hinders species i's fixation when $\rho_i < 1$ and environmental variability has no influence if $\rho_i \approx 1$. Simulation results of Fig. 8 show that ρ_i varies non-monotonically across regime (i)-(iii), with a weak dependence on the switching rate ν, and ρ_i lying between $\rho_i^{(0)}$ and $\rho_i^{(\infty)}$ for intermediate ν.

It is clear in Fig. 8 that, when there is enough environmental variance (large γ), the main effect of random switching arises at the boundary of regimes (ii)-(iii) and in regime (iii): In this case, the dichotomous noise balances the strong selection pressure yielding $\widetilde{\phi}_i < 1$ and $\rho_i < 1$ when $\widetilde{\phi}_i|_{\langle K\rangle} \approx 1$ (for $r_i < r_{i\pm1}$), and $\widetilde{\phi}_i > 0$ and $\rho_i > 1$ when $\widetilde{\phi}_i|_{\langle K\rangle} \approx 0$ (for $r_i > r_{i\pm1}$). This signals a systematic deviation from the asymptotic zero-one law predicted by the LOW in the constant-K BDCLV. The LOW and the zero-one LOW still arise in the switching-K BDCLV with $s = O(1)$, but they set in for much larger values of $\langle K\rangle$ than in the constant-K BDCLV (for $\langle K\rangle = 10^3 - 10^4$), see insets of Fig. 8. This demonstrates again that environmental variability acts to "level the field" of cyclic competition among the species by hindering the onset of the zero-one LOW.

From Eq. (29), when $s\langle K\rangle \ll 1$, to leading order, we find

$$\rho_i = 1 - s(\langle K\rangle - \kappa)\left(\frac{r_i - r_{i-1}}{12}\right), \tag{32}$$

with $\kappa = (1-\gamma^2)\langle K\rangle$ if $\nu/s \gg 1$ and $\kappa = \langle K\rangle$ if $\nu/s \ll 1$. When $s\langle K\rangle \ll 1$ and $\nu/s \gg 1$, we thus have have $\rho_i \approx 1 - s\gamma^2(r_i - r_{i-1})/12$ when $\nu/s \gg 1$ and $\rho_i = 1 + O(s^2)$ when $\nu/s \ll 1$. This means that in regime (i), and at the boundary of regimes (i)-(ii), when there is enough switching ($\nu \gg s$), $\rho_i > 1$ if $r_i < r_{i-1}$ and $\rho_i < 1$ if $r_i > r_{i-1}$, which is in agreement with the results of Fig. 8. Accordingly, whether a fast switching environment promotes/hinders species i under weak selection depends only on its growth rate relative to that of its strong opponent. In Fig. 8, we notice a non-monotonic dependence of ρ_i on $s\langle K\rangle$ resulting from a different influence of environmental variability under weak and strong selection: In Fig. 8, the fixation probability of a species that is promoted/hindered under weak selection is hindered/promoted under strong selection.

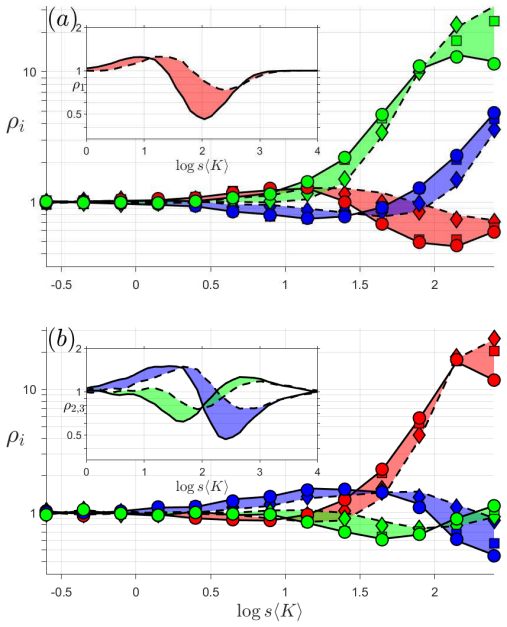

Figure 8: ρ_i vs. $s\langle K\rangle$ for values of $s \in (10^{-3}, 1)$ and with $\langle K\rangle = 250$ and $\gamma = 0.8$ kept fixed, see text. (a) $\vec{r} = \vec{r}^{(1)}$; (b) $\vec{r} = \vec{r}^{(2)}$. Shaded areas and symbols are from stochastic simulations with $\nu = 10$ ($\circ$), $\nu = 0.1$ ($\square$), $\nu = 10^{-5/2}$ ($\diamond$); lines show $\rho_i^{(\infty)}$ (fast switching, solid) and $\rho_i^{(0)}$ (slow switching, dashed), see text. Insets: (a) $\rho_1^{(\infty)}$ (solid) and $\rho_1^{(0)}$ (dashed) vs. $s\langle K\rangle$; (b) $\rho_2^{(\infty)}$ and $\rho_3^{(\infty)}$ (solid), $\rho_2^{(0)}$ and $\rho_3^{(0)}$ (dashed) vs. $s\langle K\rangle$ with $\gamma = 0.8$ and $\langle K\rangle = 10000$ fixed and s varies between $1/\langle K\rangle$ and 1. When $s\langle K\rangle = 10^3 - 10^4$, $\rho_i \to 1$. In both panels and insets: species 1 in red, species 2 in blue, and species 3 in green; $\vec{x}_0 = \vec{x}_c$; $\epsilon = 0$.

4.2. *Mean fixation time in the switching-K BDCLV*

In Sec. S5.2, we analyze the effect of random switching on the mean extinction and absorption times T_1 and T_2 characterizing respectively the stages 1 and 2 of the switching-K BDCLV dynamics, see Figs. S5 (a,b). We thus show that, when $\vec{x}_0 = \vec{x}_c$, the overall mean fixation time $T_F = T_1 + T_2 = O(\langle N\rangle) = O(\langle K\rangle)$ scales linearly with the average population size, see Fig. S5 (c), similarly to T_F in the constant-K BDCLV. Hence, random switching makes the cyclic competition more "egalitarian" but does not prolong species coexistence. We also show that the average number of switches occurring in Stage 1 scales as $\nu\langle K\rangle$, see Fig. S6 (a), while the average number environmental switches along the edge $(i, i+1)$ in Stage 2 scales as $O(\nu/\alpha_i)$ when s is neither vanishingly small nor too large.

5. Fixation properties of close-to-zero-sum rock-paper-scissors games in fluctuating populations

The general, *non-zero-sum*, rock-paper-scissors refers to the game with payoff matrix (1) where $\epsilon \neq 0$ and non-zero average fitness $\bar{f} = 1 - \epsilon \sum_{i=1}^{3} \alpha_i x_i x_{i+1}$. The mean-field description of the general RPS game, formulated as the birth-death process (5)-(7) with $0 \leq s \leq 1/(1+\epsilon)$, is given by (see Sec. S1.1)

$$\begin{aligned} \dot{N} &= N\left(\bar{f} - \frac{N}{K}\right) \\ \dot{x}_i &= x_i[\alpha_i x_{i+1} - (1+\epsilon)\alpha_{i-1}x_{i-1} + 1 - \bar{f}]. \end{aligned} \tag{33}$$

In this model, the evolution of N is coupled with the x_i's, whose mean-field dynamics is characterized by heteroclinic cycles when $\epsilon > 0$ and a stable coexistence fixed point when $\epsilon < 0$ [20, 13, 14, 16, 17, 74, 18]

In this section, we briefly focus on the fixation probabilities of close-to-zero-sum rock-paper-scissors games when $|\epsilon| \ll 1$. We therefore approximate $\bar{f} \approx 1$ and still assume that there is a timescale separation between N and x_i. This assumption is backed up by simulations results which also show that fixation properties that are *qualitatively the same* as in the BDCLV, see Fig. 9 (to be compared with Figs. 4 and 7). This suggests that the fixation probabilities of close-to-zero-sum RPS games can be obtained from those of the BDCLV by rescaling the selection intensity according to $s \to s(1 + \sigma\epsilon + O(\epsilon^2))$, see Fig. 9. To determine the parameter σ, we consider the constant-K RPS dynamics with $0 < \epsilon \ll 1$. Since the fixation properties of the BDCLV vary little with the selection intensity at quasi neutrality and under strong selection, we focus on the regime (ii) of weak selection where $s \ll 1$ and $sK = O(10)$, and assume that $\phi_{ij} \approx 1/3$ and $P_{(i,j)} \approx 1$. As shown in Sec. S3, the absorption probability of species i along the edge $(i, i+1)$ in the realm of this approximation is

$$\phi_i \simeq \frac{e^{-\alpha_i(1+\frac{\epsilon}{2})K} + \alpha_i(1+\frac{\epsilon}{2})K - 1}{\alpha_i(1+\frac{\epsilon}{2})K(1 - e^{-\alpha_i(1+\frac{\epsilon}{2})K})},$$

which coincides with (15) upon rescaling the selection intensity according $s \to s(1 + (\epsilon/2))$. Hence, if $\widetilde{\phi}_i^{\epsilon}(s)$ and $\widetilde{\phi}_i^{\mathrm{BDCLV}}(s)$ denote respectively the fixation probability of species i in close-to-zero-sum RPS game with $0 < \epsilon \ll 1$ and in the BDCLV, we have $\widetilde{\phi}_i^{\epsilon}(s) \simeq \widetilde{\phi}_i^{\mathrm{BDCLV}}(s(1 + \epsilon/2))$. Since $\widetilde{\phi}_i$ is related to $\phi_i|_K$, via (17), the overall fixation probability is also obtained by rescaling the fixation probability $\widetilde{\phi}_i^{\mathrm{BDCLV}}$ with the same carrying capacity K according to $s \to s(1 + (\epsilon/2))$. This is confirmed by the results of Fig. 9 (a) where we find that this scaling holds across the regimes (i)-(iii).

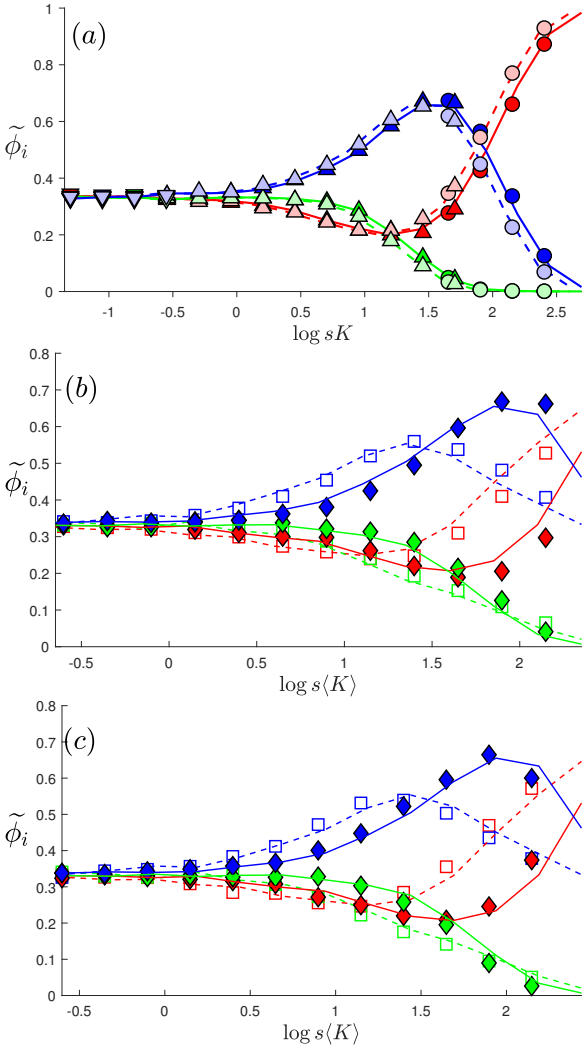

Figure 9: (a) $\widetilde{\phi}_i$ vs. sK in the close-to-zero-sum RPS game with constant carrying capacity $K = 450$ (circles), 90 (upward triangles), 50 (downward triangles), $\epsilon = -0.2$ (light symbols) and $\epsilon = 0.2$ (dark symbols). Lines show stochastic simulation results for the BDCLV ($\epsilon = 0$, see Fig. 4) with rescaled selection intensity $s \to s(1 + \epsilon/2)$ with $\epsilon = 0.2$ (solid) and $\epsilon = -0.2$ (dashed). Dark symbols / solid lines and light symbols / dashed lines collapse, demonstrating $\widetilde{\phi}_i^{\epsilon}(s) \simeq \widetilde{\phi}_i^{\mathrm{BDCLV}}(s(1 + \epsilon/2))$, see text. (b) $\widetilde{\phi}_i$ vs. $s\langle K\rangle$ when K switches between $K_- = 50$ and $K_+ = 450$ ($\langle K\rangle = 250, \gamma = 0.8$), with $s \in (10^{-3}, 1)$. Symbols are stochastic simulation results for $\epsilon = -0.2$ and and $\nu = 10$ (filled diamonds) and $\nu = 0.001$ (open squares). Lines are stochastic simulation results from the BDCLV with same switching carrying capacity, $\nu = 10$ (solid) and $\nu = 0.001$ (dashed) and rescaled selection intensity $s \to s(1 + \epsilon/2)$, see text and Fig. 7. (c) Same as in panel (b) with $\epsilon > 0$: Symbols are stochastic simulation results for $\epsilon = 0.2$; solid ($\nu = 10$) and dashed ($\nu = 0.001$) lines are results from the BDCLV with same switching carrying capacity and selection intensity $s \to s(1 + \epsilon/2)$. In all panels: red denotes species 1, blue species 2, and green species 3; $\vec{r} = \vec{r}^{(1)}$ and $\vec{x}_0 = \vec{x}_c$.

This conclusion also holds when the carrying capacity $K(t)$ is randomly switching according to (4) and $|\epsilon| \ll 1$, see Fig. 9 (b). In fact, proceeding as above and focusing on the weak selection regime where $s \ll 1$ and $sK = O(10)$, we can assume $\phi_{ij} \approx 1/3$ and $P_{(i,j)} \approx 1$, and find that ϕ_i is given by (26) with the same carrying capacity $K(t)$ and a rescaled selection intensity $s \to s(1 + (\epsilon/2))$. Along the same arguments as above, we expect that also when the carrying capacity is switching, the overall fixation probabilities across the regimes (i)-(iii) are approximately the same as in the switching-K BDCLV subject to a rescaled selection intensity $s(1 + (\epsilon/2))$. This is confirmed by the results of Fig. 9 (b) where we have reported $\widetilde{\phi}_i$ for fast and slow switching rates. As in the BDCLV, values of $\widetilde{\phi}_i$ for intermediate ν lie between the data shown in Fig. 9 (b).

In Section Sec. S5.4, we show that the mean fixation time in the BDCLV with a rescaled selection intensity $s \to s(1 + (\epsilon/2))$ allows us to obtain the mean fixation time of the close-to-zero-sum RPS game when sK and $s\langle K\rangle$ are of order $O(10)$ and $|\epsilon| \ll 1$.

6. Summary & Conclusion

Inspired by the evolution of microbial communities in volatile environments, we have studied the evolution three species engaged in a cyclic rock-paper-scissors competition when the environment varies randomly. In a static environment, the fixation probabilities in rock-paper-scissors games obey two different laws: The "law of the weakest" (LOW) prescribes that the species with the lowest payoff is the most likely to fixate in large populations, whereas a different rule ("law of stay out", LOSO) arises in smaller populations [6, 4, 5, 33]. In this work, we have studied how this simple scenario changes when environmental and demographic noise are *coupled*. Environmental randomness is here introduced via a randomly switching carrying capacity (dichotomous Markov noise) modeling how the available resources switch continuously between states of scarcity and abundance.

We have studied a birth-and-death process, in which a fluctuating population of three species competing cyclically is subject to either a constant or randomly switching carrying capacity. As demographic fluctuations (internal noise) depend on the population size which in turn varies with the switching carrying capacity, internal and environmental noise are here coupled. The size of the fluctuating population can be subject to either the LOW (weak internal noise) or the LOSO (stronger internal noise), or can switch between values subject to one and then the other law. This can greatly influence the fixation properties: It is not clear which species will be the most likely to prevail when the population size fluctuates and how the outcome depends on the environmental variability. These questions have been studied in detail for the zero-sum rock-paper-scissors game, equivalent to the cyclic Lotka-Volterra model (CLV).

The CLV dynamics consists of two stages: Species coexist in Stage 1 until one of them dies out initiating Stage 2 that consists of a two-species competition. When the carrying capacity is constant, the CLV fixation probabilities under strong selection obey the LOW and the LOSO holds under weak selection. When the CLV is subject to a randomly switching carrying capacity, the fixation probabilities can be expressed in terms of the fixation probabilities of the CLV subject to a suitable constant carrying capacity. This has allowed us to analyze in detail how the variance and rate of change of the carrying capacity affect the fixation properties of the CLV. We have found that the general effect of random switching is to balance selection, and to "level the field" of the cyclic competition: When the average carrying capacity is kept constant, the species that is the least likely to fixate has a higher probability to prevail under random switching than in a static environment. In particular, we have shown that when the rate of switching is large, the effect of the environmental noise is to effectively reduce the selection strength by a factor increasing with the variance of the carrying capacity. Hence, when the carrying capacity has a large variance, the LOW becomes a zero-one-law only for much larger average population size than in the absence of switching. We have also found new fixation scenarios, not obeying neither the LOSO nor the LOW: Under determined conditions, one of the species surviving Stage 1 is best off below a critical switching rate, whereas the other is most likely to win under faster switching. Under random switching, fixation still occurs after a mean time that scales linearly with the average of the population size, with the subleading prefactor affected by the switching rate. Hence, environmental variability renders cyclic competition more "egalitarian" but does not prolong species coexistence. Finally, we have considered close-to-zero-sum rock-paper-scissors games and have shown that the fixation probabilities can be obtained from those of the CLV by a suitable rescaling of the selection intensity.

Acknowledgments

We thank Alastair Rucklidge for many helpful discussions. The support of an EPSRC PhD studentship (Grant No. EP/N509681/1) is gratefully acknowledged.

[1] E. Pennisi, Science, **309**, 90 (2005).
[2] J. F. Crow and M. Kimura, *An Introduction to Population Genetics Theory* (Blackburn Press, New Jersey, 2009).
[3] W. J. Ewens, *Mathematical Population Genetics* (Springer, New York, 2004).
[4] M. Frean; E. D. Abraham, Proc. R. Soc. Lond. B **268**, 1323 (2001).
[5] M. Ifti and B. Bergensen, Eur. Phys. J. E, **10**, 241 (2003).
[6] M. Berr, T. Reichenbach, M. Schottenloher and E. Frey, Phys. Rev. Lett. **102**, 048102 (2009).
[7] E. Frey, Physica A, **389**, 4265 (2010).
[8] T. Reichenbach, M. Mobilia and E. Frey, Nature (London) **448**, 1046 (2007).
[9] A. Szolnoki, M. Mobilia, L.-L. Jiang, B. Szczesny, A. M. Rucklidge, and M. Perc, J. R. Soc. Interface **11**, 20140735 (2014).
[10] B. Kerr, M. A. Riley, M. W. Feldman, and B. J. M. Bohannan, Nature (London) **418**, 171 (2002).
[11] J. B. C. Jackson and L. Buss, Proc. Nat. Acad. Sci. USA, **72**, 5160 (1975).
[12] B. Sinervo and C. M. Lively, Nature (London) **380**, 240 (1996).
[13] J. Maynard Smith, *Evolution and the Theory of Games* (Cambridge University Press, Cambridge , U.K.).
[14] J. Hofbauer and K. Sigmund, K., *Evolutionary games and population dynamics* (Cambridge University Press, U.K., 1998).
[15] R. M. Nowak, *Evolutionary Dynamics* (Belknap Press, Cambridge, USA, 2006).
[16] G. Szabó and G. Fáth, Phys. Rep. **446** 97 (2007)
[17] M. Broom and J. Rychtář, *Game-Theoretical Models in Biology* (CRC Press, Boca Raton, USA, 2013).
[18] U. Dobramysl, M. Mobilia, M. Pleimling, and U. C. Täuber, J. Phys. A: Math. Theor. **51**, 063001 (2018)
[19] T. Reichenbach, M. Mobilia and E.Frey, Phys. Rev. E **74**, 051907 (2006).
[20] R. M. May and W. J. Leonard, SIAM J. Appl. Math. **29**, 243 (1975).
[21] T. Reichenbach, M. Mobilia, and E. Frey, Banach Centre Publications **80**, 259 (2008).
[22] K. I. Tainaka, Phys. Rev. Lett. **63**, 2688 (1989).
[23] K. I. Tainaka, Phys. Lett. A **176**, 303 (1993).
[24] K. I. Tainaka, Phys. Rev. E **50**, 3401 (1994).
[25] Q. He, M. Mobilia, and U. C. Täuber, Phys. Rev. E **82**, 051909 (2010).
[26] X. Ni, W. X. Wang, Y. C. Lai, and C. Grebogi, Phys. Rev. E **82**, 066211 (2010).
[27] S. Venkat and M. Pleimling, Phys. Rev. E **81**, 021917 (2010).
[28] A. Dobrinevski and E. Frey, Phys. Rev. E **85**, 051903 (2012).
[29] J. Knebel, T. Krüger, M. F. Weber, and E. Frey Phys. Rev. Lett. **110** 168106 (2013).
[30] N. Mitarai, I. Gunnarson, B. N. Pedersen, C. A. Rosiek, and K. Sneppen, Phys. Rev. E **93**, 042408 (2016).
[31] G. Szabó and A. Szolnoki, Phys. Rev. E **65**, 036115 (2002).
[32] M. Perc, A. Szolnoki, and G. Szabó, Phys. Rev. E **75**, 052102 (2007).
[33] R. West, M. Mobilia and A. M. Rucklidge, Phys. Rev. E **97**, 022406 (2018).
[34] C. A. Fux, J. W. Costerton, P. S. Stewart, and P. Stoodley, Trends Microbiol. **13**, 34 (2005).
[35] R. M. May, *Stability and Complexity in Model Ecosystems* (Princeton University Press, Princeton, New Jersey, 1974).
[36] E. Kussell, R. Kishony, N. Q. Balaban, and S. Leibler, Genetics **169**, 1807 (2005).
[37] M. Acer, J. Mettetal, and A. van Oudenaarden, Nature Genetics **40**, 471 (2008);
[38] P. Visco, R. J. Allen, S. N. Majumdar, M. R. Evans, *Biophys. J.* **98**, 1099 (2010).
[39] U. Dobramysl and U. C. Täuber, Phys. Rev. Lett. **110**, 048105 (2013).
[40] M. Assaf, E. Roberts, Z. Luthey-Schulten, and N. Goldenfeld, Phys. Rev. Lett. **111**, 058102 (2013).
[41] M. Assaf, M. Mobilia, and E. Roberts, Phys. Rev. Lett. **111**, 011134 (2013).
[42] P. Ashcroft, P. M. Altrock, and T. Galla, J. R. Soc. Interface **11**, 20140663 (2014).
[43] P. G. Hufton, Y. T. Lin, T. Galla, and A. J. McKane, Phys. Rev. E **93**, 052119 (2016).
[44] J. Hidalgo, S. Suweis, and A. Maritan, J. Theor. Biol. **413**, 1 (2017).
[45] B. Xue and S. Leibler, Phys. Rev. Lett. **119**, 108103 (2017).
[46] M. Danino and N. M. Shnerb, J. Theor. Biol. **441**, 84 (2018).
[47] P. G. Hufton, Y. T. Lin, and T. Galla, and A. J. McKane, Phys. Rev. E **99**, 032122 (2019).
[48] R. Levins, *Evolution in Changing environments: some Theoretical Explorations* (Princeton University Press, Princeton, New Jersey, 1968).
[49] J. Roughgarden, *Theory of Population Genetics and Evolutionary Ecology: An Introduction* (Macmillan, New York, 1979).
[50] J. S. Chuang, O. Rivoire, and S. Leibler S, Science **323**, 272 (2009).
[51] A. Melbinger, J. Cremer, and E. Frey, Phys. Rev. Lett. **105**, 178101 (2010).
[52] E. A. Yurtsev, H. Xiao Chao, M. S. Datta, T. Artemova, and J. Gore, Molecular Systems Biology **9**, 683 (2013).
[53] A. Sanchez and J. Gore, PLoS Biology **11**, e1001547 (2013).
[54] K. I. Harrington and A. Sanchez, Communicative & Integrative Biology **7**, e28230:1-7.
[55] A. Melbinger, J. Cremer, and E. Frey, J. R. Soc. Interface **12**, 20150171 (2015).
[56] K. Wienand, E. Frey, and M. Mobilia, Phys. Rev. Lett **119**, 158301 (2017).
[57] K. Wienand, E. Frey, and M. Mobilia, J. R. Soc. Interface **15**, 20180343 (2018).
[58] A. McAvoy, N. Fraiman, C. Hauert, J. Wakeley, and M. A. Nowak, Theor. Popul. Biol. **121**, 72 (2018).
[59] L. M. Wahl, P. J. Gerrish, and I. Saika-Voivod, Genetics **162**, 961 (2002).
[60] M. A. Brockhurst, A. Buckling, and A. Gardner, Curr. Biol. **17**, 761 (2007).
[61] Z. Patwas and L. M. Wahl, Evolution **64**, 1166 (2009).
[62] H. A. Lindsey, J. Gallie, S. Taylor, and B. Kerr, Nature (London) **494**, 463 (2013).
[63] W. Horsthemke and R. Lefever, *Noise-Induced Transitions* (Springer, Berlin, 2006).
[64] I. Bena, Int. J. Mod. Phys. B **20**, 2825 (2006).
[65] K. Kitahara, W. Horsthemke, and R. Lefever, Phys. Lett. **70A**, 377 (1979).
[66] M. H. A. Davis, J. R. Stat. Soc. B **46**, 353 (1984).
[67] J.-C. Claussen and A. Traulsen, Phys. Rev. Lett. **100**, 058104 (2008).
[68] M. Mobilia, J. Theor. Biol. **264**, 1 (2010).
[69] T. Galla, J. Theor. Biol. **269**, 46 (2011).
[70] T. Reichenbach, M. Mobilia, and E. Frey, Phys. Rev. Lett. **99**, 238105 (2007).
[71] T. Reichenbach, M. Mobilia, and E. Frey, J. Theor. Biol. **254**, 368 (2008).
[72] Q. He, M. Mobilia, and U. C. Täuber, Eur. Phys. J. B **82**, 97 (2011).
[73] B. Szczesny, M. Mobilia and A. M. Rucklidge, EPL (Europhysics Letters) **102**, 28012 (2013).
[74] B. Szczesny, M. Mobilia and A. M. Rucklidge, Phys. Rev. E **90**, 032704 (2014).

[75] M. Mobilia, A. M. Rucklidge, and B. Szczesny, Games **7**, 24 (2016).
[76] Q. Yang, T. Rogers, and J. H. P. Dawes, J. Theor. Biol. **432**, 157 (2017).
[77] C. M. Postlethwaite and A. M. Rucklidge, EPL (Europhysics Letters) **117**, 48006 (2017)
[78] P. A. P. Moran, *The statistical processes of evolutionary theory.* (Clarendon, Oxford, 1962).
[79] R. A. Blythe and A. J. McKane, J. Stat. Mech. **P07018** (2007).
[80] T. Antal and I. Scheuring, Bull. Math. Biol. **68**, 1923 (2006).
[81] C. Spalding, C. R. Doering, and G. R. Flierl, Phys. Rev. E **96**, 042411 (2017).
[82] C. Gardiner, *Handbook of Stochastic Methods* (Springer, New York, U.S.A., 2002).
[83] N. G. Van Kampen, *Stochastic Processes in Physics and Chemistry* (Elsevier, Amsterdam, Netherland, 1992).
[84] D. T. Gillespie, J. Comput. Phys. **22**, 403 (1976).
[85] Supplementary Material is electronically available at the following URL: *https://doi.org/10.6084/m9.figshare.8858273.v1*.